Materials & Design 209 (2021) 109974

Contents lists available at ScienceDirect

Materials & Design

journal homepage: www.elsevier.com/locate/matdes

Review: The effect of different nanofiller materials on the thermoelectric behavior of bismuth telluride

Farah M. El-Makaty *, Hira Khalil Ahmed, Khaled M. Youssef

Department of Materials Science and Technology, Qatar University, Doha 2713, Qatar

HIGHLIGHTS

- Nanofiller dimensionality governs the thermoelectric properties of Bi_2Te_3 composites.
- The ZT enhancement of these composites is mostly preeminent to 2D nanofillers.
- Superior thermoelectric properties are attained using doped Bi_2Te_3 matrixes.

GRAPHICAL ABSTRACT

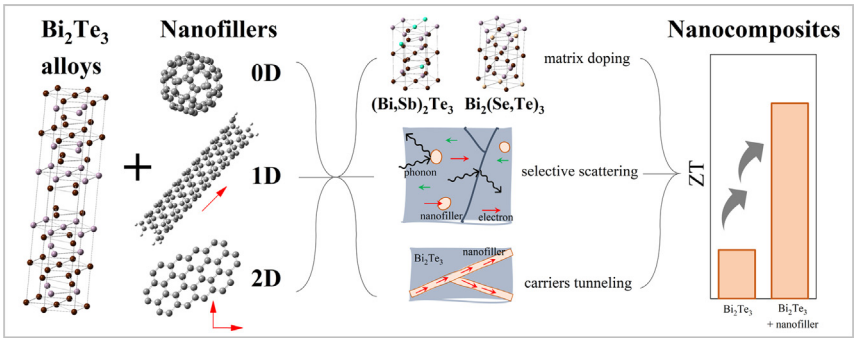

ARTICLE INFO

Article history:
Received 4 April 2021
Revised 27 June 2021
Accepted 6 July 2021
Available online 8 July 2021

Keywords:
Thermoelectric materials
Bismuth telluride
Nanofillers
Figure-of-merit
Composites

ABSTRACT

This review paper summarizes and discusses the effect of nanosized fillers on bismuth telluride nanocomposites for thermoelectric applications. Classified into various dimensions based on electron confinement in space, the nanofiller effect on the figure-of-merit value is studied. By combining experimental data with theoretical models, the mechanisms for enhancing the thermoelectric properties were proposed. The outcomes of this review paper suggest that doped bismuth telluride composites (doped with selenium for n-type or antinomy for p-type) offer better thermoelectric properties compared to undoped composites. Moreover, improvements in undoped bismuth telluride composites are exclusive for the n-type only. The figure-of-merit value for bismuth telluride composites is less than two, where the 2D nanofillers show optimum ZT improvements. Nevertheless, the inconsistency of reported data in the thermoelectric area is a problem that must be addressed to have more control over the precision of the reported results for a better understanding of the concepts in this field.

© 2021 The Author(s). Published by Elsevier Ltd. This is an open access article under the CC BY license (http://creativecommons.org/licenses/by/4.0/).

Contents

1. Introduction . . . 2
2. Compositing as a strategy for thermoelectric properties improvement . . . 3
   2.1. Matrix . . . 3
   2.2. Nanofillers . . . 3
3. Bismuth telluride-based nanocomposites . . . 4

* Corresponding author.

https://doi.org/10.1016/j.matdes.2021.109974
0264-1275/© 2021 The Author(s). Published by Elsevier Ltd.
This is an open access article under the CC BY license (http://creativecommons.org/licenses/by/4.0/).

Nomenclature

AM&P	Agate mortar and pestle
BM	Ball milling
CM	Chemical method
EGL	Expanded graphene layer
FEP	Facile electroless plating
GML	Graphene monolayer
GNP	Graphene nanoplatelets
GNS	Graphene nanosheets
HFIHS	High-frequency induction heated sintering
HP	Hot pressing
HTHP	High-temperature high-pressure synthesis
HTS	Hydrothermal synthesis
ISP	In-situ process
MS	Melt spinning
MWCNT	Multiwall carbon nanotubes
NA	Nano amorphous
ND	Nanodot
NI	Nano inclusions
NP	Nanoparticles
NPL	Nanoplatelet
NR	Nanorods
NS	Nanosheets
NW	Nanowires
PF	Power Factor
PRM	Poly reduction method
RGO	Reduced graphene oxide nanosheets
RM	Reflexing method
SAP	Self-assembly protocol
SM	Solvent mixing
SPS	Spark plasma sintering
SSR	Solid state reaction
SWCNT	Single wall carbon nanotubes
US	Ultra-sonification
VF	Vacuum filtration
WCS	Wet-chemical synthetic method

3.1. Two – Dimensional nanofillers/bismuth telluride-based nanocomposites . . . 4
3.2. One – Dimensional nanofillers/bismuth telluride-based nanocomposites. . . . 6
3.3. Zero-dimensional nanofillers/bismuth telluride-based nanocomposites . . . 6
4. Summary of optimized trends in nanofiller-based bismuth telluride nanocomposites . . . 8
5. Mechanisms for thermoelectric enhancements in bismuth telluride nanocomposites . . . 9
5.1. Matrix (Bismuth telluride) doping effect . . . 9
5.2. Selective scattering at nanofillers – Bismuth telluride matrix interfaces . . . 9
5.3. Tunneling of charge carriers . . . 10
5.4. Energy filtering effect . . . 11
6. Comparison tables . . . 11
7. Future development . . . 11
8. Challenges . . . 13
9. Conclusion . . . 13
Declaration of Competing Interest . . . 13
Acknowledgments . . . 13
References . . . 13

1. Introduction

Thermoelectric (TE) materials are promising devices for reducing energy consumption through scavenging waste heat and converting it into electrical energy. Despite the wide variety of TE materials available, bismuth-telluride-based (Bi_2Te_3) alloys present one of the most critical systems used for near room-temperature applications (T < 250 °C) [1–3]. Bi_2Te_3 alloys are currently employed in the area of medical appliances, microelectronic devices, power generation, air conditioning, transportation, and aerospace [2–4] (Fig. 1). However, the available products in these areas are limited to low-voltage devices due to the insignificant efficiencies of Bi_2Te_3 alloys. Advancements in bismuth telluride thermoelectrics have become the need of the hour in order to utilize waste heat and overcome environmental problems such as climate change and global warming.

In general, the efficiency of a TE material is governed by the magnitude of the figure-of-merit (*ZT*), which is defined as: $ZT = (S^2\sigma T)/\kappa$, where *S* is the Seebeck coefficient, σ is the electrical conductivity, *T* is the absolute temperature, and κ is the total thermal conductivity. To produce an effective TE device with a high conversion efficiency, a ZT value close to three is required [5]. However,

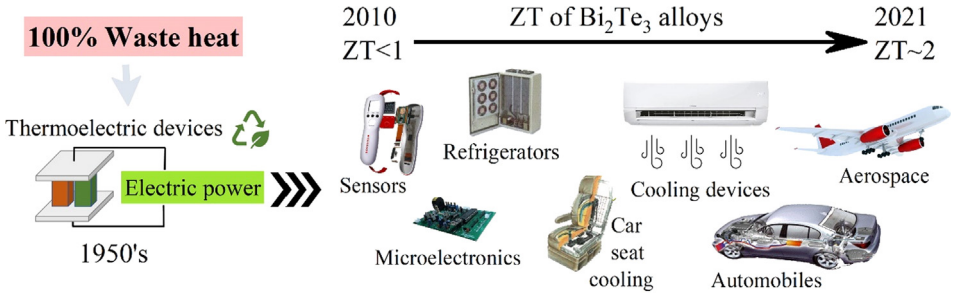

Fig. 1. Thermoelectric applications of Bi_2Te_3 alloys.

most bismuth telluride alloys fabricated have a figure-of-merit value of less than two, limiting their commercial usage [2,5].

Countless efforts have been made to enhance the TE properties of bismuth telluride alloys. However, due to the interdependence of the thermoelectric properties and the difficulty of controlling them, only marginal ZT improvements are observed. To develop a better understanding of the overall thermoelectric trends in bismuth telluride alloys and propose valid routes for improving their efficiencies, several review articles have addressed various design aspects of Bi_2Te_3 alloys. In particular, one design method that has been extensively addressed is the nanostructuring of Bi_2Te_3 alloys [6,7]. Another recent review paper summarizes the strategies employed for improving the TE properties of Bi_2Te_3, including texture alignment, nanostructuring, point defect engineering, and bandgap enlargement [8]. Other papers discussed the effect of the processing conditions [9] and the general developments made to enhance Bi_2Te_3 alloys [10].

Out of all the strategies developed for improving the efficiency of bismuth telluride alloys, nano compositing owns quite a few advantages. The preparation techniques utilized for producing the nanocomposites (e.g., ball milling, hydrothermal synthesis, compaction, etc.) are simple, low-cost approaches that can deliver the large amounts of material needed for a wide-spread of thermoelectric devices in the market. However, up to our knowledge, there are no review papers dedicated to providing comprehensive assessments on the factors affecting the thermoelectric properties of Bi_2Te_3 nanocomposites.

The aim of this review paper is to discuss the work done on the nano compositing of bismuth telluride and the subsequent effects on the thermoelectric properties. The main comparisons presented are based on the different types of nanofillers used (1D, 2D, and 3D). The outcomes of this review article are critical as they combine experimental data with theoretical models to provide an overview of the mechanisms taking place in bismuth telluride nanocomposites, examine the selection choices of the different nanofillers and matrixes used, discuss the research gaps in this field, and offer future directions for producing efficient bismuth telluride nanocomposites with high ZT values.

2. Compositing as a strategy for thermoelectric properties improvement

The addition of elements or materials into bismuth telluride results in either an alloy or a composite, and it is well-reported to be an effective way of enhancing the thermoelectric properties [11]. However, the effect of each category varies depending on the distinct microstructure formed. Fig. 2 illustrates the differences between alloys, composites, and their subgroups. To lessen the number of variables and fairly deliver critical conclusions, this review paper is limited to the nano compositing of bismuth telluride only.

Nano compositing is an innovative way of producing materials with superior properties that cannot be achieved with individual components. Nanocomposites consist of a matrix (e.g., bismuth telluride alloy) and a nanofiller. The main idea behind nano compositing is the induced selective scattering at the new interfacial areas created between the matrix and the nanofiller [12]. This feature makes it possible to reduce the thermal conductivity to a great extent without sacrificing much of the electrical properties.

2.1. Matrix

The excellent TE properties of Bi_2Te_3 alloys are a result of its layered rhombohedral structure. In the unit cell, bismuth (Bi) and tellurium (Te) layers are stacked along the c-axis, where Van der Waals bonding exists between every five atomic layers in the order Te-Bi-Te-Bi-Te [13,14] (see Fig. 3). Alloying Bi_2Te_3 with antimony ($(Bi,Sb)_2Te_3$) or selenium ($Bi_2(Te,Se)_3$) results in hole-conducting or electron-conducting TE material, respectively. Bismuth telluride alloys have good electrical performance (σ reaching 10^3 Sm/m^2) [9], large effective mass of charge carriers (0.76 m_e) [15] and low thermal conductivity (can go < 0.5 W/(m.K)) [8], making it an ideal thermoelectric material.

2.2. Nanofillers

Since the discovery of nanomaterials, it is established that the filler size could play a significant role in altering materials behavior once modified at the nanoscale (<100 nm). The exclusive properties generated at the nanoscale are due to the electron confinement in space, and they greatly depend on the material's dimensions. Moreover, based on the number of dimensions of a material that are within the nanoscale range, they are classified into different categories. Two-dimensional (2D) nanomaterials have only one dimension within the nanoscale, one-dimensional (1D) nanomaterials have two dimensions in the nanoscale, while zero-dimensional (0D) nanomaterials have all the three dimensions in the nanoscale [16].

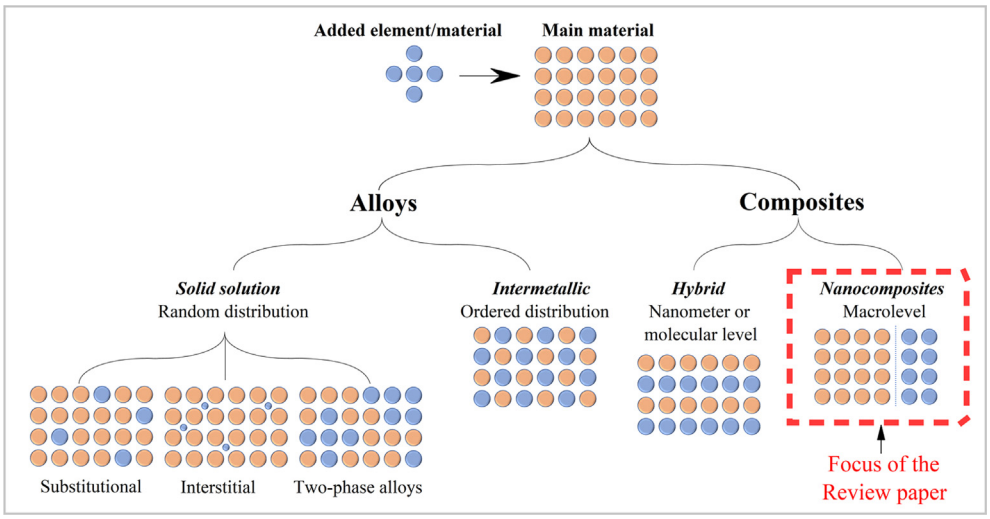

Fig. 2. Differences between alloys, composites, and their subgroups.

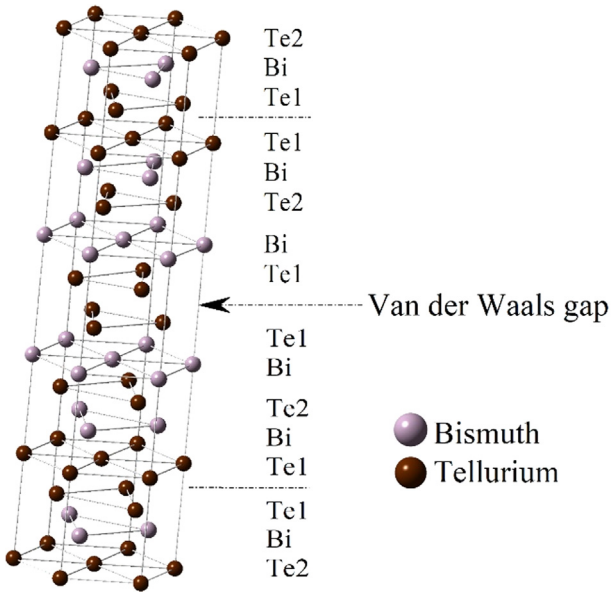

Fig. 3. The crystal structure of bismuth telluride.

The physical and chemical properties of nanofillers are distinct when compared to the same material in its bulk form. One important physical property that is greatly influenced by the nanoscale is the electrical conductivity. The motion of charge carriers within the nanofillers is restricted to certain dimensions resulting in drastic changes in the electronic transport performance. This phenomenon is known as the quantum size effect. The confinement of charge carriers in at least one dimension affects the density-of-states and energy levels as presented in Fig. 4 [17]. This feature allows for fixability in designing the electronic behavior as well as in the bandgap of nanofillers.

Another important property of nanofillers is the increased reactivity due to their small particle size accompanied by high surface area. The Van der Waal forces existing between the nanoparticles are dominant and have a high influence on the behavior of the nanofillers. As the size of the material decreases to the nanoscale, the surface area to volume ratio rises exponentially, leading to a highly interactive nanomaterial with itself (agglomeration) and with other materials (matrix within a nanocomposite) [18,19].

Other unique characteristics of nanofillers include tunneling of charge carriers, increased interfacial area, enhanced chemical reactivity, and improved adhesion forces. All the properties mentioned here make nanofillers of various dimensions an interesting candidate to study. For these reasons, a significant number of researchers have investigated the influence of nanofillers on the TE properties of bismuth telluride nanocomposites. These studies are grouped based on the dimensionality of the nanofiller (0D, 1D, and 2D) and are summarized in Sections 3 and 4. In Section 5, a comprehensive analysis of the mechanisms leading to enhancements in bismuth telluride nanocomposites is presented.

3. Bismuth telluride-based nanocomposites

This section describes the work done on nano compositing of bismuth telluride and the subsequent effect on figure-of-merit based on the various dimensions of nanofillers used.

3.1. Two – Dimensional nanofillers/bismuth telluride-based nanocomposites

For 2D nanofiller/bismuth telluride nanocomposites, most studies focused on using graphene regardless of its form (graphene monolayers, graphene nanosheets, reduced graphene oxides, and expanded graphene layers). Two other studies have investigated the addition of MXene [20] and polythiophene polymer nanosheets [21]. However, the addition of 2D nanofillers to bismuth telluride did not always improve the TE properties. Table 1 lists all the studies that attempted to enhance the thermoelectric properties using 2D nanofillers and their corresponding improvements in the ZT values.

The usage of 2D nanofillers in bismuth telluride composites revealed phenomenal results. The majority of graphene-based nanocomposites showed enhancements in ZT. Few cases where the addition of graphene did not show improvements in ZT represent the inferior concentrations in that particular study (since the same studies reported improvements in ZT for other filler concentrations as presented in the first section of Table 1). The poor filler concentrations in some cases were a result of the predominantly high amounts of graphene (3–10 wt% filler). In a study by Ju and Kim [24], high concentrations of RGO caused a reduction in the Seebeck coefficient due to the bipolar effect. Other reasons for the low ZT are increased thermal conductivity after graphene addition, as noticed by Liang et al. [4], and low electrical conductivity due to agglomeration and carrier scattering as observed by Zhang et al. [30]. Hence, adding graphene enhances the ZT of bismuth telluride nanocomposites, but optimization of the filler content is mandatory.

On another note, the nanocomposite prepared by Lu et al. [20] presented the first evidence of remarkable improvement in the thermoelectric properties through employing MXene (a transition carbide, $Ti_3C_2T_x$) as a 2D nanofiller. However, the usage of polythiophene nanosheets as a filler by Ao et al. [21] resulted in exceptionally low electrical conductivity and Seebeck coefficient values due to the poor conductivity of the organic polymer, hence a low ZT.

Enhancement in the figure-of-merit values using 2D fillers is incredible. Using graphene with undoped Bi_2Te_3 alloy showed improvements ranging from 25% up to 587%. Only one study investigated the effect of graphene addition to doped n-type $Bi_2(Te,Se)_3$ matrix and showed 100% improvement in ZT, reaching a final value of 0.8. For doped p-type $(Bi.Sb)_2Te_3$ nanocomposites, the maximum improvement was 53%. However, all the composites resulted in an

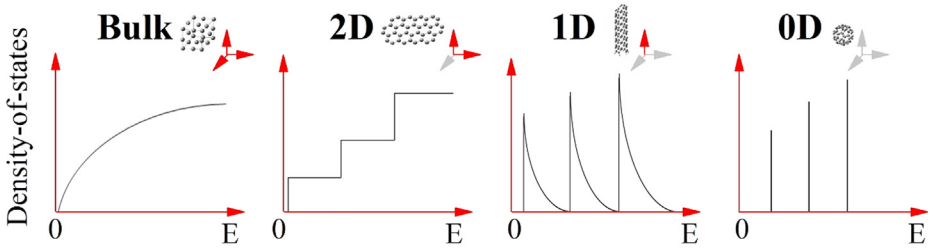

Fig. 4. The electronic density-of-states based on the dimensionality of the filler.

Table 1
2D nanofiller/bismuth telluride nanocomposites.

Matrix (type)	Type	Filler	Filler content	Optimum filler content	Mixing method	Temperature range (K)	Optimum improvement in ZT (improvement at RT)	Reference (year)
Improved cases								
Bi_2Te_3	n	GML	0 – 0.05 wt%	0.05 wt%	AM&P and pressed	300 – 480	0.68 → 0.92 at 402 K	[22] (2016)
Bi_2Te_3	n	GNS	0, 0.5, 0.75 and 1.5 vol%	1.5 vol%	US, BM, pressed and sintered	300 – 525	0.08 → 0.55 at 500 K (0.1 → 0.29)	[23] (2018)
Bi_2Te_3	n	GNS	0 and 0.2 vol%	0.2 vol%	HTS and SPS	300 – 480	0.16 → 0.21 at 475 K (0.1 → 0.14)	[4] (2013)
Bi_2Te_3	n	GNS	0 and 5 vol%	5 vol%	SSR, pressed and sintered	5–350	(0.3 → 0.45)	[13] (2010)
Bi_2Te_3	n	RGO	0, 0.5 and 1 wt%	1 wt%	WCS, pressed and sintered	300	(0.24 → 0.3)	[24] (2016)
Bi_2Te_3 (NW)	n	RGO	0, 0.5, 1 and 3 wt%	1 wt%	WCS, pressed and sintered	300	(0.31 → 0.4)	[24] (2016)
Bi_2Te_3 (NW)	n	RGO	0, 0.5, 1, 3, 5 and 10 wt%	0.5 wt%	WCS, pressed and sintered	PF: 600 → 688.9 uW/mk^2 at 300 K		[25] (2015)
Bi_2Te_3 (NS)	n	RGO	Without & with graphene	with graphene	RM and pressed	300–380	0.22 → 0.35 at 343 K (0.12 → 0.23)	[26] (2018)
Bi_2Te_3	n	RGO	0, 0.25, 5 and 1 wt%	0.25 wt%	US and HP	PF: 1267 → 1329 uW/mk^2 at 423 K		[27] (2019)
$Bi_2Te_{2.7}Se_{0.3}$	n	GNS	0, 0.05 and 0.5 wt%	0.05 wt%	BM and SPS	300–573	0.4 → 0.81 at 433 K (0.66 → 0.5)	[28] (2021)
$Bi_{0.4}Sb_{1.6}Te_3$	p	GNS	0, 0.1, 0.2, 0.3 and 0.4 vol%	0.4 vol%	CM and HP	300–498	1.34 → 1.54 at 440 K (1 → 1.1)	[29] (2015)
$Bi_{0.4}Sb_{1.6}Te_3$	p	GNS	0, 0.02 and 0.05 wt%	0.05 wt%	BM and HPHT	323–500	1.09 → 1.26 at 423 K (0.96 → 1.13)	[30] (2017)
$Bi_{0.48}Sb_{1.52}Te_3$	p	GNS	0, 0.05, 0.1 and 0.15 wt%	0.05 wt%	ZM and SPS	300–550	0.9 → 1.25 at 320 K (0.85 → 1.2)	[31] (2016)
$Bi_{0.5}Sb_{1.5}Te_3$	p	GNP	0, and 0.5 vol%	0.5 vol%	BM and HFIHS	300 – 475	0.89 → 1.2 370 (0.71 → 0.95)	[32] (2019)
$Bi_{0.36}Sb_{1.64}Te_3$ (NR)	p	RGO	0, 0.1, 0.4 and 0.8 vol%	0.4 vol%	MS and SPS	300–473	1 → 1.16 at 393 K (0.8 → 0.98)	[33] (2017)
$Bi_{0.5}Sb_{1.5}Te_3$ (NPL)	p	EGL	0, 0.1, 0.3 and 0.5 vol%	0.1 vol%	BM and SPS	300 – 480	0.74 → 1.13 at 360 K (0.7 → 1)	[34] (2015)
$Bi_{0.4}Sb_{1.6}Te_3$	p	MXene	0, 0.5, 1 and 2 vol%	1 vo1.%	SAP and SPS	300–475	1.13 → 1.3 at 400 K (1 → 1.16)	[20] (2020)
Unimproved cases								
Bi_2Te_3	n	GNS	0, 0.1 and 2 vol%	–	HTS and SPS	300 – 480	–	[4] (2013)
Bi_2Te_3	n	RGO	0, 3, 5 and 10 wt%	–	WCS, pressed and sintered	300	–	[24] (2016)
Bi_2Te_3 (NW)	n	RGO	0, 5 and 10 wt%	–	WCS, pressed and sintered	300	–	[24] (2016)
Bi_2Te_3 (NP)	n	Polythiophene nanosheets	0, 5, 20, 25, 30 and 40 wt%	–	AM&P and SPS	300–473	–	[21] (2011)
$Bi_{0.4}Sb_{1.6}Te_3$	p	GNS	0 and 0.1 wt%	–	BM and HPHT	323–500	–	[30] (2017)
$Bi_{0.5}Sb_{1.5}Te_3$	p	GNP	0 and 1 vol%	–	BM and HFIHS	300–475	–	[32] (2019)

Table 2
1D nanofiller/bismuth telluride nanocomposites.

Matrix	Type	Filler	Filler content	Optimum filler content	Mixing method	Temperature range (K)	Optimum improvement in ZT (improvement at RT)	Reference (year)
Improved cases								
Bi_2Te_3	n	SWCNT (L = 0.5–2 um, d = 0.7–1,4 nm)	0 and 0.5 wt%	0.5 wt%	AM&P, pressed and sintered	2 – 340 K	0.99 → 1.28 at 282 K (1 → 1.24)	[38] (2012)
Bi_2Te_3	n	SWCNT (L = 1–10 um, d = 2–10 nm)	0, 0.5, 0.75, 1 and 1.5 vol%	0.5 vol%	US, pressed and HFIHS	300 – 525 K	0.087 → 0.53 at 420 K (0.092–0.32)	[39] (2017)
Bi_2Te_3	n	MWCNT	0 and 0.7 wt%	0.7 wt%	CM and SPS	298 – 498 K	0.52 → 0.85 at 473 K (0.28 → 0.48)	[40] (2012)
Bi_2Te_3	n	MWCNT (L = 2–3 um, d = 20 nm)	0 and 1 wt%	1 wt%	PRM and SPS	298–473 K	0.52 → 0.79 at 473 K (0.28 → 0.47)	[41] (2014)
Bi_2Te_3	n	MWCNT	0 and 1 wt%	1 wt%	HTS and pressed	295–340 K	0.24 → 0.36 at 333 K (0.21 → 0.29)	[42] (2017)
Bi_2Te_3	n	MWCNT (L = 10 ≥ um, d = 10–15 nm)	0, 0.36, 0.8, 3.2, 7 and 22.3 wt%	0.8 wt%	US in ethanol, and pressed	PF: 130 → 140 uW/mk^2 at 300 K		[43] (2013)
Bi_2Te_3	n	AgNW (L = 50 um, d = 50 nm)	0, 0.5, 1, 1.5, 2 and 2.5 vol%	1.5 vol%	US and SPS	300–475 K	0.16 → 0.71 at 475 K (0.11 → 0.31)	[35] (2014)
$Bi_2(Se,Te)_3$	n	MWCNT (L = 2–3 um, d = 20 nm)	0 and 1 wt%	1 wt%	PRM and SPS	298–473 K	0.52 → 0.93 at 473 K (0.28 → 0.51)	[41] (2014)
$Bi_2Te_{2.7}Se_{0.3}$	n	MWCNT (L = 1–2 um, d = 30–40 nm)	0, 0.01, 0.015, 0.03 and 0.15 vol%	0.015 vol%	BM and HP	298 – 473 K	0.88 → 0.98 at 423 K (0.57 → 0.62)	[44] (2011)
$Bi_{0.4}Sb_{1.6}Te_3$	p	MWCNT	0 and 0.05 vol%	0.05 vol%	BM and HP	298 K	(0.0037 → 0.00352)	[45] (2011)
$Bi_{0.4}Sb_{1.6}Te_3$	p	MWCNT	0, 0.5 and 1 wt%	1 wt%	BM and HP	325 – 498 K	1 → 1.1at 347 K	[46] (2013)
$Bi_{0.4}Sb_{1.6}Te_3$	p	MWCNT	0, 0.012, 0.12 and 0.15 wt%	0.12 wt%	BM and HP	298 – 473 K	1.03 → 1.47at 378 K (0.93 → 1.41)	[47] (2014)
Unimproved cases								
Bi_2Te_3	n	SWCNT (L = 5 μm, d = 6–9 nm)	0, 0.15 and 0.3 wt%	–	US, BM, pressed, and sintered	303 K	–	[48] (2018)
Bi_2Te_3	n	Rice-like polyaniline	With and without polyaniline	–	BM and pressed	300–400 K	–	[37] (2011)
Bi_2Te_3	p	SWCNT (L = 0.5–2 um, d = 0.7–1,4 nm)	0, 1 and 5 wt%	–	AM&P pressed, and sintered	2 – 340 K	–	[38] (2012)
$(Bi,Sb)_2Te_3$	p	SWCNT (L = 5–30 um, d = 1–3 nm)	0, 0.5, 1.0, and 1.5 vol%	–	BM, pressed and HFIHS	300 – 500 K	–	[49] (2017)
$Bi_{0.4}Sb_{1.6}Te_3$	p	MWCNT	0, 0.15 and 0.25 wt%	–	BM and HP	298 K	–	[45] (2012)
$Bi_{0.5}Sb_{1.5}Te_3$	p	ZnO NR	0 and 2 wt%	–	BM, pressed and sintered	300–500 K	–	[36] (2017)

optimum figure-of-merit value that was greater than 1 as their base alloy had high ZT values initially. Moreover, using MXene as a nanofiller showed an improvement of 15%, reaching a final ZT value of 1.3. The effective usage of MXene presented a great potential of utilizing a new 2D material (other than graphene) in this field. The discussed figure-of-merit improvements prove that 2D nanofillers are an effective addition for enhancing the TE behavior of bismuth telluride nanocomposites.

3.2. One – Dimensional nanofillers/bismuth telluride-based nanocomposites

For 1D nanofillers, almost all studies focused on carbon nanotubes, either single or multiwall. Three other studies have explored different 1D nanomaterials, which are silver nanowires [35], zinc oxide nanoribbons [36], and rice-like polyaniline [37]. Table 2 summarizes 1D nanofillers-bismuth telluride nanocomposites and their consequent effect on the ZT value.

Enhancements in the figure-of-merit values are quite noticeable for 1D filler composites where the majority of the cases utilized CNTs. By using MWCNT with undoped Bi_2Te_3 matrix, different research groups obtained >50% improvement for the optimum filler content obtained in each case [40–42]. However, their final ZT values were all less than one as the base alloy had low ZT values of 0.52 [40,41] and 0.24 [42]. Other studies used the same filler with doped n-type $Bi_2(Te,Se)_3$ matrixes, but their enhancement in ZT was diverse. Park et al. [44] obtained a final ZT of 0.98 for the optimum filler content (0.015 vol%), getting only 11% enhancement compared to the pristine sample. However, Kim et al. [41] had a 78% improvement starting with a lower ZT value for the matrix (0.52), reaching a comparable ZT value of 0.93. Three more groups used a doped p-type $(Bi,Sb)_2Te_3$ matrix with the same filler as well. Even though all three groups produced their nanocomposites via ball milling (different conditions), only one group had a noticeable improvement of 42% and ZT > 1 [47], while others barely had an improvement [45,46]. In a single case where MWCNTs were used, a reduction in ZT is noticed for the high filler concentrations only [45].

Few other studies used SWCNT as a 1D nanofiller, and out of the five cases, only two showed improvements in ZT. In these two studies, Zhang et al. [38] got an improvement of 29%, reaching a ZT > 1, while Ahmed et al. [39] reached 500% improvements obtaining a low final ZT of 0.53 due to the poor ZT of the base material. Other cases that showed a reduction in ZT used SWCNT with undoped Bi_2Te_3 matrixes (n- and p-types) and noticed a significant drop in electrical conductivity. A study used a doped p-type $(Bi,Sb)_2Te_3$ matrix and their reduction in ZT was due to the diminished carrier concentrations [49].

Furthermore, Zhang et al. [35] obtained an outstanding ZT improvement of 343% using silver nanowires but reached a maximum ZT value of 0.71. The remaining categories of 1D nanofillers (ZnO NR and rice-like polyaniline) had a large bandgap which lowered the electrical conductivity greatly, resulting in no improvement in ZT values. Compared to 2D, general trends depict that 2D nanofillers could reach higher overall ZT values than 1D.

3.3. Zero-dimensional nanofillers/bismuth telluride-based nanocomposites

Numerous 0D fillers have been utilized for bismuth telluride nanocompositing. Most of these nanofillers are focused on carbon (C) [22,48,50–55], silicon (Si) [56–62], and alumina (Al_2O_3) [45,63–65] nanoparticles. Other nanoparticles used include Ag [66,67], B [68], $CuGaTe_2$ [69], Fe_2O_3 [70], Fe-85Ni [70], LaFeSi [71], Ni [72], Sb_2O_3 [73], Ta_2O_5 [74], TeO_2 [75], TiC [76] and ZnO [77]. Table 3 presents a summary of the studied 0D fillers-

Table 3
Zero-dimensional nanofillers/bismuth telluride nanocomposites.

Matrix	Type	Filler	Filler content	Optimum filler content	Mixing method	Temperature range (K)	Optimum improvement in ZT (improvement at RT)	Reference (year)
Improved cases								
Bi_2Te_3	n	Ag NP	0, 0.5, 1, 1.5, 2, 2.5 and 5 vol%	2 vol%	CM and SPS	300–480 K	0.19 → 0.77at 475 K	[66] (2015)
Bi_2Te_3	n	Al_2O_3 NP	0 and 0.3 vol%	0.3 vol%	PRM and SPS	300 – 500 K	(0.16 → 0.2)	[63] (2012)
Bi_2Te_3	n	SiC NP	0, 0.1 and 0.5 wt%	0.1 wt%	BM and SPS	340–580 K	0.56 → 0.66at 440 K	[60] (2006)
$Bi_2(Te,Se)_3$	n	Al_2O_3 NP	0 and 0.5 vol%	0.5 vol%	BM and HP	300 – 525 K	0.0029 → 0.0035 at 350 K	[45] (2012)
$Bi_2Te_{2.3}Se_{0.7}$	n	Ni NP	0 and 0.4 mol.%	0.4 mol.%	US and HP	300 – 525 K	0.47 → 0.66 at 425 K (0.28 → 0.45)	[72] (2019)
$Bi_{0.5}Sb_{1.5}Te_3$	p	Al_2O_3 NP	0, 0.3, 0.5 and 1 vol%	0.3 vol%	BM and SPS	293–473 K	0.97 → 1.44 at 323 K	[64] (2013)
$Bi_{0.5}Sb_{1.5}Te_3$	p	Ag NP	0.03 and 0.05 wt%	0.03 wt%	FEP and SPS	300–500 K	0.55 → 1.07 at 373 K (0.61 → 0.95)	[67] (2017)
$Bi_{0.5}Sb_{1.5}Te_3$	p	B NA	0, 0.03, 0.04 and 0.06 wt%	0.04 wt%	BM and SPS	300 – 545 K	1.04 → 1.76 at 395 K (1.05 → 1.56)	[68] (2020)
$Bi_{0.5}Sb_{1.5}Te_3$	p	C NP	0 and 1 wt%	1 wt%	HTS, pressed and sintered	15.4 uW/mk^2 8.3 → 15.4		[50] (2012)
$(Bi,Sb)_2Te_3$	p	C60	0, 0.5, 5 vol%	0.5 vol%	BM and SPS	0–300 K	0.77 → 1.02 at 295 K	[52] (2012)
$Bi_{0.5}Sb_{1.5}Te_3$	p	C60	0, 0.5, 1.5, 1.7 and 3 vol%	0.5 vol%	BM, pressed and sintered	300–600 K	0.45 → 1.16 at 460 K	[51] (2011)
$Bi_{0.4}Sb_{1.6}Te_3$	P	$CuGaTe_2$ NI	0, 0.2, 0.4 and 0.6 vol%	0.4 wt%	BM and HP	300 – 487 K	1.02 → 1.53 at 487 K	[69] (2019)
$Bi_{0.3}Sb_{1.7}Te_3$	p	LaFeSi NP	0, 0.1, 0.2, 0.3 and 0.4 wt%	0.2 wt%	US, pressed and sintered	300 – 500 K	0.99 → 1.10 at 379 K (0.79 → 0.87)	[71] (2021)
$Bi_{0.5}Sb_{1.5}Te_3$	p	Sb_2O_3 NP	0,1, 2, 4 and 6 wt%	4 wt%	BM and SPS	300–475 K	1.15 → 1.52 350 K (1.17 → 1.38)	[73] (2018)
$Bi_{0.4}Sb_{1.6}Te_3$	p	Si NP	0, 0.3, 1 and 3 vol%	1 vol%	BM and HP	300–375 K	1.08 → 1.32 at 350 K (0.98 → 1.18)	[61] (2014)
$Bi_{0.4}Sb_{1.6}Te_3$	p	Si NI	0 and 0.5 vol%	0.5 vol%	BM and SPS	300 – 500 K	1.31 → 1.36 at 423 K	[62] (2020)
$Bi_{0.5}Sb_{1.5}Te_3$	p	SiC NP	0, 0.05, 0.1, 0.2, 0.5, 1, 2 and 5 vol%	0.1 vol%	BM and SPS	323 – 473 K	0.88 → 0.97 at 323 K	[57] (2010)
$Bi_{0.3}Sb_{1.7}Te_3$	p	SiC NP	0, 0.1, 0.3, 0.4 and 0.6 vol%	0.4 vol%	BM and SPS	300 – 500 K	1.22 → 1.33 at 373 K (1.1 → 1.25)	[58] (2013)
$(Bi,Sb)_2Te_3$	p	Si_3N_4 NA	0, 0.22, 0.44 and 0.88 vol%	0.44 vol%	BM and SPS	303–483 K	1.28 → 1.37 at 383 K (1.01 → 1.20)	[59] (2015)
$Bi_{0.4}Sb_{1.6}Te_3$	p	SiO_2 NA	0, 0.55, 1.1 and 2.2 vol%	0.55 vol%	BM and SPS	293 – 390 K	1.15 → 1.27 at 363 K (0.88 → 1.12)	[56] (2013)
$Bi_{0.5}Sb_{1.5}Te_3$	p	Ta_2O_5 NP	0, 2 and 4 wt%	4 wt%	BM and SPS	300–450 K	(1.1 → 1.38)	[74] (2017)
$Bi_{0.5}Sb_{1.5}Te_3$	p	TeO_2 NP	0 and 3 wt%	3 wt%	BM and SPS	300–400 K	0.92 → 1.07 at 350 K (0.71 → 0.98)	[75] (2018)
$Bi_{0.5}Sb_{1.5}Te_3$	p	ZnO NI	5 vol%	5 vol%	BM and SPS	300 – 500 K	0.98 → 1.28 at 340 K (0.95 → 1.12)	[77] (2016)
Unimproved cases								
Bi_2Te_3	n	C60	0 and 7.5 vol%	–	BM and HP	210 – 298 K	–	[53] (2011)
Bi_2Te_3	n	C NA	0, 0.15 and 0.30 wt%	–	US, BM, pressed and sintered	30C	–	[48] (2017)
Bi_2Te_3	n	Graphite	0 and 0.05 wt%	–	AM&P and pressed	300 – 480 K	–	[22] (2016)
$Bi_2Te_{2.7}Se_{0.3}$	n	SiC NP	0, 0.05, 0.1, 0.2, 0.5 and 1 vol%	–	BM and SPS	323 – 473 k	–	[57] (2010)
$Bi_2Te_{2.7}Se_{0.3}$	n	ZnO NI	5 vol%	–	BM and SPS	300–500 K	–	[77] (2016)
Bi_2Te_3	p	C60	0, 2, 7.5 and 20 vol%	–	BM and HP	140 – 298 K	–	[53] (2011)
$Bi_{0.5}Sb_{1.5}Te_3$	p	Al_2O_3 NP	0, 2 ,4 and 6 wt%	–	BM and SPS	300 – 500 K	–	[65] (2019)
$(Bi,Sb)_2Te_3$	p	C60	0, 1, 8 wt%	–	BM and SPS	300 K	–	[55] (2010)
$Bi_{0.4}Sb_{1.6}Te_3$	p	C60 NI	0, 1 and 8 mol.%	–	BM and HP	10–300 K	–	[54] (2009)
$Bi_{0.4}Sb_{1.6}Te_3$	p	C60 NI	0, 0.01, 0.1, 1,5,8 and 10 mol.%	–	BM and HP	10–300 K	–	[54] (2009)
$Bi_{0.5}Sb_{1.5}Te_3$	p	Fe_2O_3 NP	2 wt%	–	BM and SPS	300–400 K	–	[70] (2016)
$Bi_{0.5}Sb_{1.5}Te_3$	p	Fe-85Ni NP	2 wt%	–	BM and SPS	300–400 K	–	[70] (2016)
$Bi_{0.4}Sb_{1.6}Te_3$	p	Si NI	0, 0.1 and 1.5 vol%	–	BM and SPS	300 – 500 K	–	[62] (2020)
$Bi_{0.5}Sb_{1.5}Te_3$	p	TiC NP	0, 1 and 2 wt%	–	BM and SPS	300 – 500 K	–	[76] (2019)

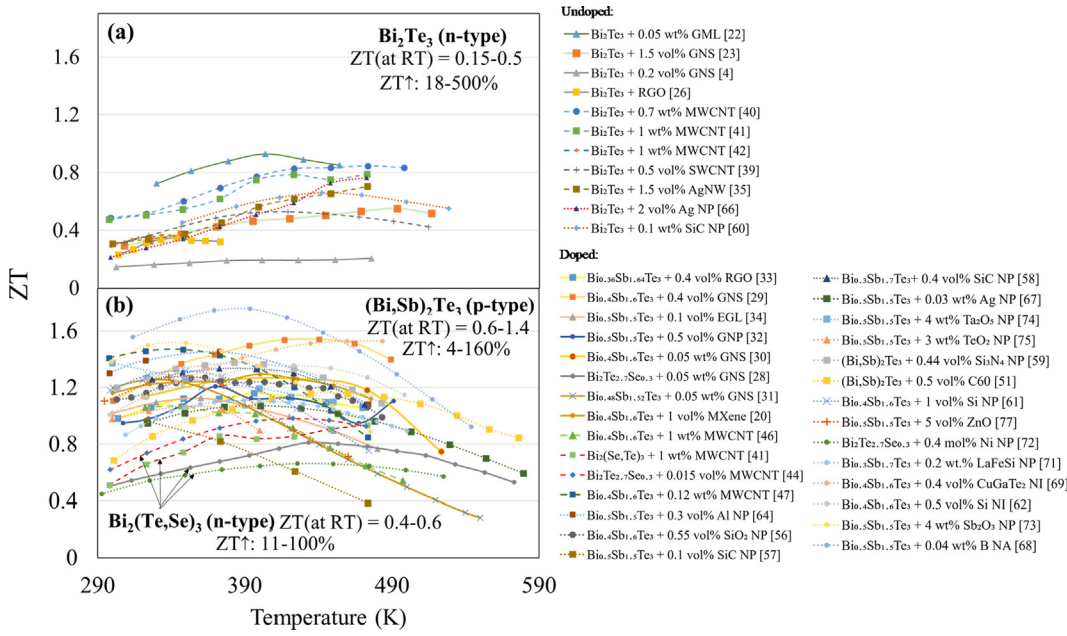

Fig. 5. Figure-of-merit trends for (a) undoped Bi_2Te_3 and (b) doped $(Bi,Sb)_2Te_3$ and $Bi_2(Te,Se)_3$ nanocomposites (ZT↑: ZT % enhancements compared to pristine due to nanofiller addition, solid line: 2D, dashed line: 1D and dotted line: 0D nanofillers).

bismuth telluride nanocomposites and their resulted effect on the ZT values.

Decent enhancements in the figure-of-merit values were observed for 0D-based nanocomposites. The highest percentage increase of 305% was observed when Zhang et al. [66] used Ag NP as a filler, but the maximum value of ZT was only 0.77 since the undoped matrix used had a low initial ZT [66]. Another group also investigated Ag NP but with a doped p-type matrix and got a higher ZT of 1.07 (95% enhancement). The following general trends were also observed in the improved cases; Si-based nanofillers displayed only average improvements of 4–22%, Al_2O_3 had better enhancements ranging from 21 – 50%, however, the highest enhancements of 32–158% were obtained when carbon was utilized. Moreover, nano-amorphous B had 65% improvement, $CuGaTe_2$ showed 50%, Ni NP 40%, while the remaining nanofillers had average enhancements ranging from 11 to 32%.

On the other hand, several 0D carbon fillers used showed deterioration in ZT values [22,48,53–55]. Some studies used fullerene nano-inclusions as a filler and showed a reduction in the ZT due to phonon blocking and trapping of electrons in the conduction band [53–55]. Furthermore, a reduction in the ZT was observed when graphite powder and amorphous carbon were used, resulting in low carrier concentrations and hence low electrical conductivity of the prepared nanocomposites [22,48]. Most other fillers which did not show enhancement in the ZT are a result of poor filler concentrations selected since using the same filler by the same group with other concentrations showed enhancement. Meanwhile, the only 0D filler that did not show improvements despite the concentration used are TiC nanoparticles.

4. Summary of optimized trends in nanofiller-based bismuth telluride nanocomposites

Fig. 5a and b summarize the optimized trends for ZT as a function of temperature for undoped and doped bismuth telluride nanocomposites, respectively. In general, doped composites showed much higher ZT values at room temperature ($(Bi,Sb)_2Te_3$/$Bi_2(Te,Se)_3$: 0.4–1.4) compared to undoped composites (Bi_2Te_3: 0.15–0.5). As shown in Fig. 5a, all optimized bismuth telluride nanocomposites after filler addition for the undoped matrix are n-type. Furthermore, Fig. 5b shows that few of the improved doped composites are n-type, while the rest are p-type. Even though the figure-of-merit trends for doped n-type (ZT at RT: 0.4–0.6) are lower than the p-type (ZT at RT: 0.6–1.4), they showed better behavior compared to undoped n-type Bi_2Te_3 (ZT at RT: 0.15–0.5).

In order to understand the effect of nanofiller shape on the thermoelectric properties of bismuth telluride nanocomposites, carbon-based bismuth telluride nanocomposites were categorized according to filler dimension and are shown in Fig. 6. Only one material (carbon) was chosen to have a fair judgment on the ZT trends and eliminate the effect of the material type. Moreover, almost all 2D and 1D fillers used by the studies are based on carbon (graphene or CNTs). Several articles have used 0D carbon nanofiller; hence a good number of references are included for comparison. It should be noted that the included references are the ones that showed improvement upon filler addition and their ZT temperature measurements ranged from 300 to 550 K. The main con-

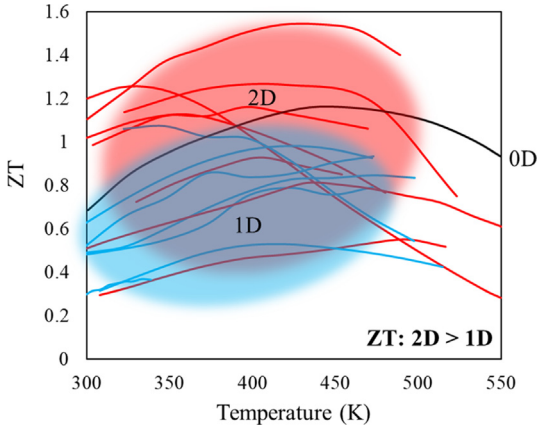

Fig. 6. Combined ZT trends for carbon/bismuth telluride-based nanocomposites highlighting the highest concentration of trends for 2D (red), 1D (blue), and 0D (gray) carbon nanofillers. (For interpretation of the references to colour in this figure legend, the reader is referred to the web version of this article.)

clusion made from Fig. 6 is that 2D carbon-based nanofillers showed higher ZT values compared to 1D. In Section 5, a detailed discussion about the mechanisms for enhancing the thermoelectric properties of bismuth telluride nanocomposites is made by engaging theoretical models with the summarized experimental data.

5. Mechanisms for thermoelectric enhancements in bismuth telluride nanocomposites

Based on the collected data for bismuth telluride nanocomposites, the following mechanisms for enhancing the thermoelectric properties were observed.

5.1. Matrix (Bismuth telluride) doping effect

Doping is the factor that had the most influence on the thermoelectric properties of bismuth telluride nanocomposites leading to a clear divergence in their trends. As noted from Fig. 5, the figure-of-merit values for doped nanocomposites ranged from 0.4 to 1.4 at room temperature, which is higher than the undoped nanocomposites where their values ranged from 0.15 to 0.5 at the same temperature. This is mainly because undoped bismuth telluride has a small bandgap of 0.14 eV resulting in the undesirable bipolar effect of minority charge carriers [78]. In order to ensure a high Seebeck coefficient value within the nanocomposite, a single type of charge carriers (either electrons or holes) should stay [79]. This is achieved by doping bismuth telluride (with Sb for the p-type or Se for the n-type) to increase the bandgap of the alloy and diminish the bipolar effect. Alloying also increases the charge carrier's concentration yielding improved electrical properties. These reasons are possible explanations of why doped nanocomposites possess higher thermoelectric properties compared to undoped ones.

On another note, the doping effect of Sb and Se on the thermoelectric properties of bismuth telluride is not alike. In p-type doping, Sb atoms sit in Bi sites with no preference, leading to more isotropic behavior of the alloy. Meanwhile, when bismuth telluride is doped as an n-type, Se atoms are selective for Te2 sites, which are the sites where Te atoms are only bonded to Bi (see Fig. 3) [8]. This selective behavior of Se atoms causes high anisotropy in the transport properties of the doped n-type, making it hard to achieve full thermoelectric properties without extra alignment processing. This may explain why doped p-type bismuth telluride nanocomposites showed superior enhancements in ZT compared to doped n-type.

Another important finding is that undoped bismuth telluride nanocomposites, which displayed improvement in the figure-of-merit values, exhibited n-type semiconductor behavior. There were no studies where undoped p-type bismuth telluride showed improvements in ZT, regardless of the dimension of the nanofiller used. This can be explained by two main reasons. The first reason is the processing technique used to prepare Bi_2Te_3 matrixes. Dannangoda et al. [80] reported that to have an undoped Bi_2Te_3 of a p-type conductor, long-range ordering of the structure should be maintained, while a defect-rich structure leads to an n-type conducting material. However, defect-rich nanostructured Bi_2Te_3 matrixes (resulted from the preparation process of the matrix, e.g., ball milling, melt spinning, etc.) are preferably used to enhance the scattering events (which enhances the ZT) and due to their processing advantages (simple, fewer impurities, low-cost, et.) compared to other preparation techniques. These defect-rich preparation processes tend to cause a transition from p-type to n-type conduction for this material due to the dominance of Te deficiencies which act as electron donors [8,80].

The second reason why undoped p-type Bi_2Te_3 did not show improvement in the ZT is the high bipolar effect. In a study conducted by Zhang et al. [38], when the undoped n-type bismuth telluride (0 and 0.5 wt% MWCNT) was tuned to p-type by increasing the concentration of 1D filler (to 1 and 5 wt%), a significant reduction in the ZT value was observed (see Fig. 7). This reduction resulted from the cancellation of the negative charge of the original Bi_2Te_3 matrix by the positive charge induced through SWCNT addition [80]. The added positive charge carriers also increased the overall carrier concentration, which in return raised the thermal conductivity of the nanocomposite. Hence, tuning the undoped n-type Bi_2Te_3 to p-type through nanofiller addition results in an undesirable combination of reduced Seebeck coefficient and increased thermal conductivity, leading to a diminished figure-of-merit value. It can be deduced that detailed compositional (e.g., doping) and structural (e.g., defects due to processing) characteristics play an important role in deciding the thermoelectric performance of undoped bismuth telluride nanocomposites.

5.2. Selective scattering at nanofillers – Bismuth telluride matrix interfaces

The key mechanism for enhancing the thermoelectric properties in bismuth telluride nanocomposites is selective scattering at the interface between the nanofiller and bismuth telluride matrix. The addition of a nanofiller causes selective scattering of phonons while allowing electrons (of shorter mean free paths) to pass [17]. This phenomenon results in a drop in the lattice thermal conductivity (the only parameter not affected by the electronic structure), while maintaining high electrical conductivity of the material. Reduction in the lattice thermal conductivity upon filler addition to bismuth telluride matrix is a given (the main reason behind nano compositing strategy). However, the drop in the thermal conductivity varies for each nanofiller type.

A theoretical model to calculate the thermal conductivity based on the filler shape within a nanocomposite has been reported. By combining Fourier's law with the effective medium theory, Siddiqui et al. [81] proposed the "generalized effective medium theory for the determination of the effective thermal conductivity of particulate nanocomposites with multiple inclusions." The proposed model considered the main nanofiller variables which affect the nanocomposite's thermal conductivity, including the filler's shape, size, distribution, and orientation. Interestingly, the formulated theory also accounted for randomly oriented 1D and 2D nanofillers within a matrix, which perfectly represents the data in this review paper. According to the model, the effective thermal conductivity of a nanocomposite can be determined by the following equation:

$$K_{eff} = \frac{\langle q\rangle_{11}\langle \nabla T\rangle_{11} + \langle q\rangle_{22}\langle \nabla T\rangle_{22} + \langle q\rangle_{33}\langle \nabla T\rangle_{33}}{\langle \nabla T\rangle_{11}{}^2 + \langle \nabla T\rangle_{22}{}^2 + \langle \nabla T\rangle_{33}{}^2}, \langle * \rangle = \frac{1}{|V|}\int_V * dV \quad (1)$$

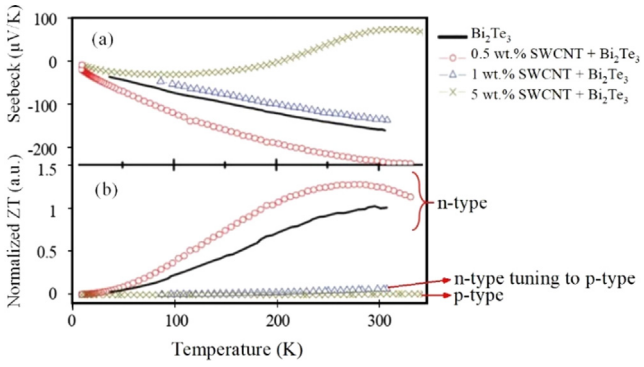

Fig. 7. (a) Seebeck and (b) ZT plots showing how tuning Bi_2Te_3 + SWCNT nanocomposite into p-type diminishes the ZT value [38].

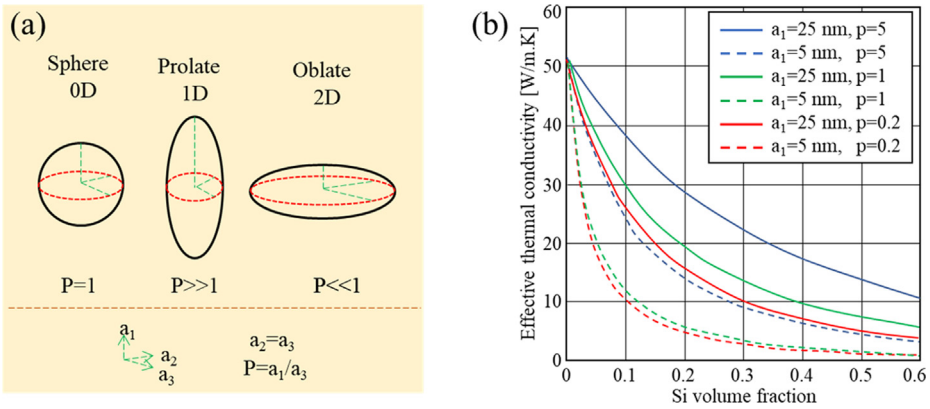

Fig. 8. (a) Si nano inclusion shapes' assumptions for the investigated model by Siddiqui et al. (b) simulated effective thermal conductivity trends for spherical, randomly oriented prolate, and randomly oriented oblate Si nano inclusions [81].

where q is the heat flux, ∇T is the temperature gradient, and V is the domain volume. A detailed derivation of the model and its explanation can be found in the reference [81]. The reference also includes comparisons made by the authors between the simulated model and experimental data as well as theoretical models developed by other groups proving its accuracy. Additionally, the authors simulated a remarkable model for Ge-Si nanocomposite and revealed significant findings. They calculated the effective thermal conductivity of Si nano inclusions in three different cases: assuming spherical shape or 0D with an aspect ratio of p = 1, prolate or 1D with $p \gg 1$, and oblate or 2D with $p \ll 1$ (see Fig. 8a). The effective thermal conductivity was investigated for these shapes with different sizes and orientations. Fig. 8b shows the application of the proposed model on spherical, randomly oriented prolate, and randomly oriented oblate Si nano inclusions of two different sizes, a = 5 and 25 nm.

It was found that nanocomposites with oblate shape (2D, p = 0.2, red lines) had the lowest effective thermal conductivity, followed by spherical (0D, p = 1, green lines), while prolate nano inclusions (1D, p = 5, blue lines) had the highest thermal conductivity. The findings of this model are in good agreement with the experimental results collected for carbon-based nanocomposites summarized in Fig. 6 (as the thermal conductivity is inversely proportional to the figure-of-merit). The justification for lower thermal conductivity in 2D compared to 1D can be explained by more interfaces existing in a 2D material, where phonons are scattered by a single nanosheet in two different dimensions, whereas in 1D, the scattering occurs from interacting with one dimension. Another important factor to consider is the alignment of nanofillers. For 0D nanofillers, scattering from all sides is the same, unlike 1D and 2D fillers (where scattering depends on the alignment of the filler). Even though the data in Fig. 6 for 0D are not enough to explicitly discuss whether 0D is better than 1D or inferior to 2D in a certain material, the theoretical simulation by Siddiqui et al. for the effect of thermal conductivity supports a similar trend. More research should be done to explain the behavior of 0D. Nevertheless, it can be concluded from the discussed data that selective scattering at the interfaces between the nanofillers and bismuth telluride is the main mechanism for improving the thermoelectric properties in bismuth telluride nanocomposites.

5.3. Tunneling of charge carriers

Another mechanism that occurs in bismuth telluride nanocomposites is the tunneling of charge carriers (also referred as the bridging or percolation effect). Tunneling is the creation of nanofiller networks for the transfer of electrical carriers. Interestingly, tunneling is consistently reported as a mechanism to enhance the electrical conductivity in 2D nanofillers-bismuth telluride nanocomposites. Kumar et al. [26] used RGO along with 2D Bi_2Te_3 nanosheets creating conducting channels leading to enhanced mobility. Ahmed et al. [23] suggested that tunneling of charge carriers had a noticeable influence on the values of electrical conductivity in their studied composite. However, several cases of using graphene as a 2D nanofillers have reported low values of electrical conductivity in some of the filler concentrations used, implying that graphene addition does not always cause tunneling of the charge carriers.

For better understanding, a proposed analytical model by Payandehpeyman et al. [82] was explored. The model is based on the mean-field theory for estimating electrical conductivity via a tunneling mechanism for randomly dispersed graphene nanosheets within a nonconductive matrix (Fig. 9). The model considers various factors, including the size, thickness, and conductivity of graphene, potential barrier height of the matrix, and tunneling distance. It is noteworthy that the model has been verified by the authors to fit well with experimental data.

The main outcome of the model is that the ultimate factor determining the initiation of tunneling effect within a graphene-based nanocomposite is the aspect ratio (d/L). According to the model, electrical conductivity increases via a tunneling effect when the aspect ratio is high. Hence, in the case of agglomerated graphene (high thickness), the aspect ratio decreases due to fewer interconnections between the 2D nanofiller resulting in a low electrical conductivity. Meanwhile, a high aspect ratio is obtained when the length of graphene increases, improving the possibility of electron tunneling through graphene nanosheets [82]. This can explain why in some cases of increased graphene's concentration (highly associated with agglomeration [83]), led to lower conductivity in the graphene-based bismuth telluride nanocomposites

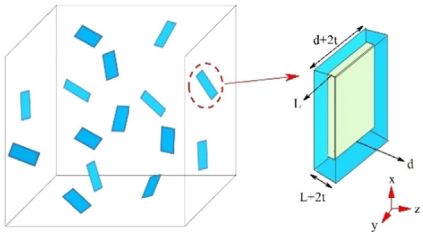

Fig. 9. Simulated model for a composite with randomly dispersed graphene nanoplatelets of a cross section d and a thickness L, surrounded by a thin interphase layer of t thickness [82].

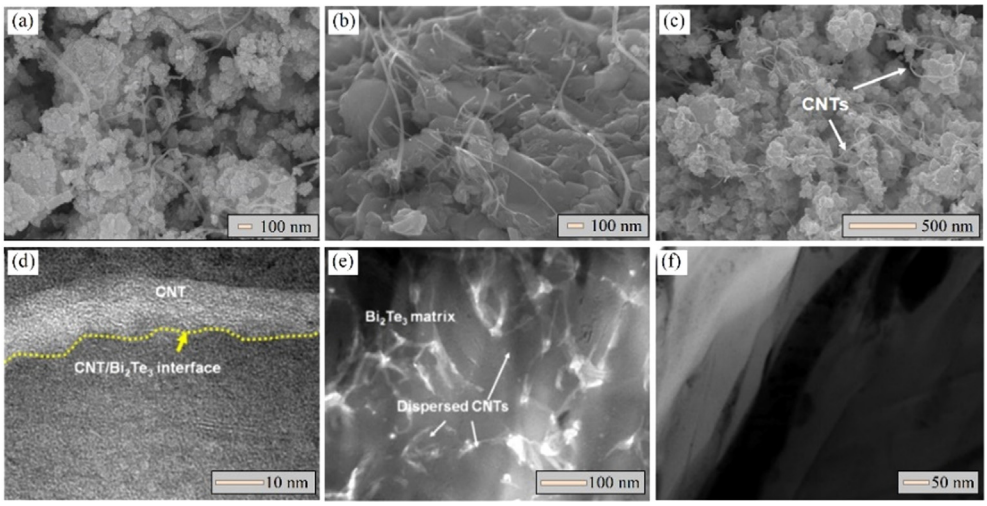

Fig. 10. SEM images showing entangled and bent behavior of CNTs in (a) $Bi_2(Se,Te)_3$/MWCNT [41], (b) $(Bi,Sb)_2Te_3$/SWCNT [49], (c) Bi_2Te_3/MWCNT [40], (d-e) low magnification TEM images of CNT/BiTe [40] and (f) TEM for AgNWs/BiTe nanocomposites [35].

[30,34]. Hence, for tunneling to take place in 2D-based nanocomposites, optimization of the filler content is mandatory to achieve high aspect ratios.

On the other hand, based on the summarized studies of bismuth telluride nanocomposites (Table 2), the tunneling mechanism fails to apply most of the time for 1D nanofillers as 11 out of the 14 references exhibited a reduction in the electrical conductivity upon filler addition. This experimental outcome can be explained by a theoretical model developed by Zare et al. [84]. The developed model calculates the theoretical electrical conductivity and percolation threshold (minimum filler concentration to obtain tunneling) in CNT-based nanocomposites. The suggested electrical conductivity model for CNT-nanocomposite is:

$$\sigma = \sigma_0 \exp\left(-\frac{4.8uR^2}{z\varphi_{eff}{}^{l}}\right) \quad (2)$$

where σ_o is a parameter, u is the waviness of CNT (u = 1 for straight and u > 1 for bent/entangled CNT), R is the radius of CNT, z is the characteristic tunneling length, l is the length of the CNT, and φ_{eff} is the percolation threshold. The conclusion of this model, confirmed by the authors through comparison with experimental data, is that the highest electrical conductivity for a CNT-based nanocomposite can be obtained when using (i) a high concentration of thin CNT, (ii) low CNT waviness with a thick interface, and (iii) short tunneling distance with high characteristic tunneling length. Out of these, it is noticed that condition (ii) does not apply for most of the 1D-bismuth telluride nanocomposites reported cases. Fig. 10 shows SEM and TEM images for different 1D-bismuth telluride nanocomposites revealing a high amount of entangling and bending in the CNTs within the bismuth telluride nanocomposites.

One main reason for the high waviness in 1D nanofillers can be attributed to the mixing process used to prepare bismuth telluride nanocomposites. Obtaining a straight 1D structure is almost impossible with techniques like ball milling and ultra-sonification, which were mostly employed to prepare these nanocomposites. According to Zare et al. [84], the waviness of CNTs lowers their effective length resulting in poor characteristics of the conductive networks. On another note, one of the few studies that showed enhancements in electrical conductivity with 1D nanofiller is by Kumar et al. [42]. The authors used a modified hydrothermal process in which the MWCNTs were used as a substrate for preparing the nanocomposite leading to enhanced carrier mobility of 17%. Thus, the preparation technique plays a critical role in creating the tunneling behavior within the 1D nanofillers and determining the electrical conductivity of 1D-bismuth telluride nanocomposites. These reasons provide additional justification for the trends in Fig. 6, were due to the tunneling mechanism in 2D nanofillers and its absence from 1D nanofillers, higher electrical conductivity and ZT values are obtained in 2D bismuth telluride nanocomposites.

Another important aspect to consider is the partial confinement of charge carriers in 1D and 2D nanofillers resulted from the density-of-states (refer to Fig. 4). For 2D nanomaterials, the confinement of electrons is in one dimension only; hence the charge carriers are free to spread in two dimensions leading to higher mobility within the tunneling networks. Meanwhile, on top of the entanglement of CNTs due to the preparation processes, the limitation of movements of charge carriers to one dimension further restricts the tunneling behavior in the 1D-bismuth telluride nanocomposites.

5.4. Energy filtering effect

Another mechanism for improving the thermoelectric properties in bismuth telluride nanocomposites is through the energy filtering effect. It is proved that nanofillers can filter low-energy charge carriers, which greatly enhances the Seebeck coefficient due to the elimination of the bipolar effect. However, by filtering out the low-energy carriers and reducing the number of charge carriers, the electrical conductivity is lowered significantly [17]. Hence, the effect of energy filtering on enhancing the ZT of thermoelectric materials is quite debatable, but it is important to mention that this effect exists in nano compositing even if it does not play a dominant part in most cases.

6. Comparison tables

This section provides a comparison for the performance of the involved systems and ranks the thermoelectric performance in each type accordingly. Table 4 presents a comparison between the bismuth telluride matrixes used (undoped, doped, n-type, and p-type), while Table 5 deals with the nanofiller types (0D, 1D, and 2D).

Table 4
Bismuth telluride matrixes comparison.

Matrix type	Conduction type	Summary	ZT (1-highest, 4-lowest)
Bi_2Te_3	n-type	-Defect-rich structure. -Can be produced via simple processing techniques. -Addition of n-type conducting fillers can enhance the electrical conductivity and Seebeck coefficient greatly.	3
	p-type	-Long-range ordered structure is required. -Difficult to obtain with regular nano compositing techniques. -Tunning the matrix to p-type through filler addition will cause a huge drop in the Seebeck coefficient.	4
$Bi_2(Te,Se)_3$	n-type	-Enhanced thermoelectric properties due to doping. -High anisotropy due to the selective behavior of Se. -Extra processing is required to achieve full thermoelectric properties.	2
$(Bi,Sb)_2Te_3$	p-type	-Enhanced thermoelectric properties due to doping. -Higher isotropy as Sb doping is not selective. -Can be produced via simple processing techniques.	1

Table 5
Nanofiller type comparison.

Filler type	Summary	ZT (1-highest, 4-lowest)
2D	-Improved scattering events due to two-dimensional interface scattering of a single sheet leading to high reductions in thermal conductivity. -Electrons are free to move in two directions, which improves tunneling behavior. -Requires optimization of the nanofiller concentration to avoid agglomeration and obtain the high aspect ratio needed for tunneling to take place. -Promising 2D nanofillers include graphene and MXene.	1
1D	-Waviness of the filler is the main factor affecting the thermoelectric properties. -Straight 1D nanofillers are difficult to obtain via the common nano compositing methods. -Less scattering events due to one-dimensional interface scattering. -Electrons are free to move in one direction only. -Tunneling is less likely to occur due to the high waviness of 1D fillers produced. -Promising 2D nanofillers include CNTs and Ag NW.	3
0D	-Not affected by the alignment of nanoparticles. -Total quantum confinement leads to charge carriers being trapped in the conduction band. -Improvements in ZT are quite noticeable in many cases. -Theoretically, scattering events in 0D are higher than 1D nanofillers. -Further investigations are required to obtain better understandings of the mechanisms affecting 0D nanofillers.	2

7. Future development

The ease of preparation and production of bismuth-telluride nanocomposites makes them a promising candidate for developing sustainable thermoelectric devices for commercial applications. Yet, the thermoelectric performance should be addressed thoroughly in order to enhance their efficiencies. Herein, some future development suggestions to improve the design of bismuth-telluride nanocomposites:

1- For enhancement in ZT values of bismuth telluride nanocomposites, the focus should be more on 2D materials as they are the most promising nanofillers. MXene represents a new good candidate that needs further studying. In addition to its exceptional electrical conductivity, MXene provides an amazing feature of tunable properties due to the infinite possibilities of altering its structure and composition. This means that endless promising options are available to investigate. However, the research of MXene as a nanofiller for bismuth telluride composites is rather limited.
2- Another promising 2D candidate to investigate is Ag nanosheets. Several studies explored the effect of 0D and 1D Ag nanofillers and showed a high percentage of enhancements (95–434%). According to Fig. 6, using the same material in 2D form is expected to have superior properties. However, it is noteworthy that the production of Ag nanosheets is quite challenging as the synthesized Ag nanosheets are usually of a high thickness (few nanometers), which is expected to lower the tunneling effect as discussed in Section 5.3. Yet, a recent study was able to successfully prepare ultrathin ($1 \leq$ nm) Ag nanosheets [85]. If utilized properly, these ultrathin Ag nanosheets are expected to produce high figure-of-merit values in bismuth-telluride nanocomposites.
3- The alignment and content of graphene nanosheets are reported to affect the thermal conductivity [86–88] and the microstructural features [89–91] of the final composite. Hence, optimizing the filler content and studying the effect of alignment is a must to achieve the maximum enhancements possible.
4- Improving the usage of 1D nanofillers requires a reduction in the waviness to boost the electrical conductivity and achieve enhancements in ZT. This is expected to be achieved through improving the preparation techniques for such composites.
5- If the main aim is to improve thermoelectric properties, doped bismuth-telluride matrixes are recommended and nano compositing of differently doped matrixes [92] are yet to be investigated.
6- Special attention to the n-type counterpart should be given, and the anisotropic behavior should be addressed through further processing of the composite to reach the advances made in the p-type conductors.
7- The behavior of 0D carbon nanofiller is still not clear. The cases of reduced ZT upon 0D carbon addition are much more than the cases where improvements were obtained. Hence,

more work is needed to develop a further understanding of the mechanisms taking place in 0D fillers.

8- Using two nanofillers of different dimensionality in the same matrix is reported to show interesting microscopic features [93], and can be an interesting route to investigate in thermoelectrics.

9- Utilizing optimized synthesis techniques in nano compositing should further improve the thermoelectric properties. Reported optimization conditions for different synthesis techniques can be found in the references [94–97].

10- One main reason for the low ZT in nanocomposites (compared to other strategies used) is the need for pressing the prepared powders. Even though nano compositing owns several industrial advantages and is more commercially feasible, the electrical conductivity of the samples is greatly affected by the density of the final product. Improvements in the compaction techniques for more efficient nano compositing production should be taken into consideration. In this regard, a recent review article by Hu et al. [98] provides an overview of the SPS technique suggesting its superior advantages in compacting thermoelectric materials due to the reduced densification temperature and short sintering time. Hence, optimizing the parameters of such a technique through engaging the reported analysis may help in enhancing the thermoelectric properties of the nanocomposites. Optimization for other consolidation techniques can be found in the references [99,100].

8. Challenges

One main difficulty faced in compiling this review was the inconsistency of the reported data. A full understanding of the TE properties requires a comprehensive study in which different parameters are properly controlled and optimized. Many studies, for example, used ball milling as a technique for the preparation of the composite. However, a difference in one parameter, such as the milling time or the base powder used, resulted in different TE trends. Another factor to consider is the various initial ZT values of the matrix in each case prior to compositing, which makes the comparison between percentage enhancements in the figure-of-merit values somehow unfair. However, the effect of matrix doping (the main factor affecting the ZT of the initial matrix) has been addressed to help evaluating the data. Moreover, critical details were missing in many articles, including the preparation methods of bismuth telluride matrix, detailed information on the nanofiller used, comprehensive identification of the microstructure of the matrix, filler, composite, and thorough information about the TE measuring devices used. A comparison between the enhancements for the different composites is difficult due to these inconsistencies. It is also noteworthy that the measuring error in both electrical and thermal conductivities is high, especially because they depend on the final density of the compacted samples and the accuracy of the devices used. However, the presented data has certain trends that are supported by theoretical models, implying that the overall conclusions made in this review are quite creditable. Nevertheless, there is a need to request authors to report all experimental details precisely to obtain clear and correct comparisons between the reported TE properties in future work.

9. Conclusion

This review paper studies the effect of different dimensional nanofillers on the TE properties of bismuth telluride-based nanocomposites. Compared to other strategies used, nano compositing offers the benefits of being cost-effective, yielding innovative materials, and provides practical products. Noticeable TE enhancements in bismuth telluride nanocomposites were achieved via the following mechanisms (i) great reduction of thermal conductivity via nanofiller-matrix selective scattering, (ii) increased electrical conductivity through tunneling effect, (iii) increased carrier concentrations for doped matrixes, and (iv) improved isotropy in the case of doped p-type. The most critical outcomes of this review paper are (i) undoped matrixes showed improvements only for the n-type conduction, (ii) doped matrixes showed better enhancements in the p-type compared to the n-type, and (iii) for a certain nanofiller material type, 2D nanofillers have significant ZT improvements compared to 1D nanofillers. These results offer a better understanding of the nano compositing effects in bismuth telluride alloys and provide specific directions to consider in future work. Some of the obtained outcomes about nanofillers can be extended and applied in different thermoelectric materials having a similar structure to bismuth telluride, hence it allows for improving the strategy of nano compositing to produce various innovative thermoelectric materials.

CRediT authorship contribution statement

Farah Elmakaty: Writing - Original Draft, Visualization, Conceptualization, Investigation, Formal analysis, Software. **Hira Khalil:** Writing - Original Draft, Software, Investigation, Visualization. **Khaled Youssef:** Writing - Review & Editing, Conceptualization, Supervision, Project administration, Funding acquisition.

Declaration of Competing Interest

The authors declare that they have no known competing financial interests or personal relationships that could have appeared to influence the work reported in this paper.

Acknowledgments

This work was supported by Grant no. NPRP10–0206–170366 from Qatar National Research Fund (a member of the Qatar Foundation). The statements made herein are solely the responsibility of the authors. Open access publication of this article was funded by the Qatar National Library.

References

[1] A. Nozariasbmarz, B. Poudel, W. Li, H.B. Kang, H. Zhu, S. Priya, Bismuth telluride thermoelectrics with 8% module efficiency for waste heat recovery application, iScience 23 (2020) 101340, https://doi.org/10.1016/j.isci.2020.101340.

[2] G. Tan, M. Ohta, M. Kanatzidis, Thermoelectric power generation: From new materials to devices, Philosophical Transactions of the Royal Society A: Mathematical, Physical and Engineering Sciences 377 (2019) 20180450, https://doi.org/10.1098/rsta.2018.0450.

[3] M.G. Kanatzidis, Nanostructured thermoelectrics: The new paradigm?, 22 (2010) 648-659, 10.1021/cm902195j.

[4] B. Liang, Z. Song, M. Wang, L. Wang, W. Jiang, Fabrication and thermoelectric properties of graphene/bi2te3 composite materials, (2013), 10.1155/2013/210767.

[5] M. Rull, A. Moure, J. Fernández, M. Martín-González, Skutterudites as thermoelectric materials: Revisited, RSC Adv. 5 (2015), https://doi.org/10.1039/C5RA03942H.

[6] H. Mamur, M.R.A. Bhuiyan, F. Korkmaz, M. Nil, A review on bismuth telluride (bi2te3) nanostructure for thermoelectric applications, Renew. Sustain. Energy Rev. 82 (2018) 4159–4169, https://doi.org/10.1016/j.rser.2017.10.112.

[7] E. Ashalley, H. Chen, X. Tong, H. Li, Z. Wang, Bismuth telluride nanostructures: Preparation, thermoelectric properties and topological insulating effect, Frontiers of Materials Science 9 (2015), https://doi.org/10.1007/s11706-015-0285-9.

[8] M. Hong, Z.-G. Chen, J. Zou, Fundamental and progress of bi2te3-based thermoelectric materials, Chin. Phys. B 27 (2018), https://doi.org/10.1088/1674-1056/27/4/048403 048403.

[9] H.J. Goldsmid, Bismuth telluride and its alloys as materials for thermoelectric generation, Materials (Basel, Switzerland) 7 (2014) 2577–2592, https://doi.org/10.3390/ma7042577.
[10] Y. Chen, X. Hou, C. Ma, Y. Dou, W. Wu, Review of development status of bi2te3-based semiconductor thermoelectric power generation, (2018) 1-9, https://doi.org/10.1155/2018/1210562.
[11] D. Beretta, N. Neophytou, J.M. Hodges, M.G. Kanatzidis, D. Narducci, M. Martin- Gonzalez, M. Beekman, B. Balke, G. Cerretti, W. Tremel, A. Zevalkink, A.I. Hofmann, C. Müller, B. Dörling, M. Campoy-Quiles, M. Caironi, Thermoelectrics: From history, a window to the future, Materials Science and Engineering: R: Reports 138 (2019) 100501, https://doi.org/10.1016/j.mser.2018.09.001.
[12] M. Alsalama, H. Hamoudi, K.M. Youssef, The effect of graphene structural integrity on the power factor of tin selenide nanocomposite, J. Alloy. Compd. 159584 (2021), https://doi.org/10.1016/j.jallcom.2021.159584.
[13] A.H. Li, M. Shahbazi, S.H. Zhou, G.X. Wang, C. Zhang, P. Jood, G. Peleckis, Y. Du, Z.X. Cheng, X.L. Wang, Y.K. Kuo, Electronic structure and thermoelectric properties of bi2te3 crystals and graphene-doped bi2te3, Thin Solid Films 518 (2010) e57–e60, https://doi.org/10.1016/j.tsf.2010.03.124.
[14] H. An, M. Pusko, D. Chun, S. Park, J. Moon, In-situ synthesis of flexible hybrid composite films for improved thermoelectric performance, Chem. Eng. J. 357 (2019) 547–558, https://doi.org/10.1016/j.cej.2018.09.200.
[15] C. Lee, J.N. Kim, J.-Y. Tak, H.K. Cho, J.H. Shim, Y.S. Lim, M.-H. Whangbo, Comparison of the electronic and thermoelectric properties of three layered phases bi2te3, pbbi2te4 and pbbi4te7: Lego thermoelectrics, AIP Adv. 8 (2018), https://doi.org/10.1063/1.5047823 115213.
[16] J. Orton, in: Semiconductors and the Information Revolution, ed J. Orton (Academic Press, Amsterdam, 2009).
[17] Q. Zhu, S. Wang, X. Wang, A. Suwardi, M.H. Chua, X.Y.D. Soo, J. Xu, Bottom-up engineering strategies for high-performance thermoelectric materials, Nano-Micro Letters 13 (2021) 119, https://doi.org/10.1007/s40820-021-00637-z.
[18] U. Szeluga, S. Pusz, B. Kumanek, K. Olszowska, A. Kobyliukh, B. Trzebicka, Effect of graphene filler structure on electrical, thermal, mechanical, and fire retardant properties of epoxy-graphene nanocomposites - a review, Critical Reviews in Solid State & Materials Science 46 (2021) 152–187, https://doi.org/10.1080/10408436.2019.1708702.
[19] E.I. Akpan, X. Shen, B. Wetzel, K. Friedrich, in: Polymer composites with functionalized nanoparticles, eds K. Pielichowski, T.M. Majka (Elsevier, 2019).
[20] X. Lu, Q. Zhang, J. Liao, H. Chen, Y. Fan, J. Xing, S. Gu, J. Huang, J. Ma, J. Wang, L. Wang, W. Jiang, High-efficiency thermoelectric power generation enabled by homogeneous incorporation of mxene in (bi, sb)2te3 matrix, Adv. Energy Mater. 10 (2020) 1902986, https://doi.org/10.1002/aenm.201902986.
[21] W. Ao, L. Wang, J. Li, F. Pan, C. Wu, Synthesis and characterization of polythiophene/bite nanocomposite thermoelectric material, J. Electron. Mater. 40 (2011) 2027, https://doi.org/10.1007/s11664-011-1664-3.
[22] K. Agarwal, V. Kaushik, D. Varandani, A. Dhar, B.R. Mehta, Nanoscale thermoelectric properties of bi2te3 – graphene nanocomposites: Conducting atomic force, scanning thermal and kelvin probe microscopy studies, J. Alloy. Compd. 681 (2016) 394–401, https://doi.org/10.1016/j.jallcom.2016.04.161.
[23] K. Ahmad, C. Wan, M.A. Al-Eshaikh, A.N. Kadachi, Full length article: Enhanced thermoelectric performance of bi2te3 based graphene nanocomposites, Appl. Surf. Sci. (2018), https://doi.org/10.1016/j.apsusc.2018.10.163.
[24] H. Ju, J. Kim, Preparation and structure dependent thermoelectric properties of nanostructured bulk bismuth telluride with graphene, J. Alloy. Compd. 664 (2016) 639–647, https://doi.org/10.1016/j.jallcom.2016.01.002.
[25] H. Ju, M. Kim, J. Kim, Preparation of graphene sheets into one-dimensionally nanostructured bulk bismuth telluride for enhancing thermoelectric power factor, 27 (2016) 3427-3434, 10.1007/s10854-015-4175-9.
[26] S. Kumar, S. Singh, P.K. Dhawan, R.R. Yadav, N. Khare, Effect of graphene nanofillers on the enhanced thermoelectric properties of bi2te3 nanosheets: Elucidating the role of interface in de-coupling the electrical and thermal characteristics, 29 (2018), 10.1088/1361-6528/aaa99e.
[27] Y. Du, J. Li, J. Xu, P. Eklund, Thermoelectric properties of reduced graphene oxide/bi2te3 nanocomposites 12 (2019) 2430, https://doi.org/10.3390/en12122430.
[28] F.M. El-Makaty, K. Andre Mkhoyan, K.M. Youssef, The effects of structural integrity of graphene on the thermoelectric properties of the n-type bismuth-telluride alloy, Journal of Alloys and Compounds 876 160198 (2021), https://doi.org/10.1016/j.jallcom.2021.160198.
[29] C. Li, X. Qin, Y. Li, D. Li, J. Zhang, H. Guo, H. Xin, C. Song, Simultaneous increase in conductivity and phonon scattering in a graphene nanosheets/(bi2te3)0.2(sb2te3)0.8 thermoelectric nanocomposite, Journal of Alloys and Compounds 661 (2016) 389–395, https://doi.org/10.1016/j.jallcom.2015.11.217.
[30] Y. Zhang, H. Ma, B. Sun, B. Liu, H. Liu, L. Kong, B. Liu, X. Jia, X. Chen, Thermoelectric performance of graphene composited bisbte bulks by high pressure synthesis, J. Alloy. Compd. 715 (2017) 344–348, https://doi.org/10.1016/j.jallcom.2017.05.004.
[31] X. Dewen, X. Jingtao, L. Guoqiang, L. Zhu, S. Hezhu, T. Xiaojian, J. Jun, J. Haochuan, Synergistic optimization of thermoelectric performance in p-type bi0.48sb1.52te3/graphene composite, 9 (2016) 236-244, 10.3390/en9040236.
[32] K. Ahmad, C. Wan, P.-A. Zong, Thermoelectric properties of bisbte/graphene nanocomposites, J. Mater. Sci.: Mater. Electron. 30 (2019) 11923–11930, https://doi.org/10.1007/s10854-019-01538-z.
[33] W.H. Shin, K. Ahn, M. Jeong, J.S. Yoon, J.M. Song, S. Lee, W.S. Seo, Y.S. Lim, Enhanced thermoelectric performance of reduced graphene oxide incorporated bismuth-antimony-telluride by lattice thermal conductivity reduction, J. Alloy. Compd. 718 (2017) 342–348, https://doi.org/10.1016/j.jallcom.2017.05.204.
[34] D. Suh, S. Lee, H. Mun, S.-H. Park, K.H. Lee, S. Wng Kim, J.-Y. Choi, S. Baik, Enhanced thermoelectric performance of bi0.5sb1.5te3-expanded graphene composites by simultaneous modulation of electronic and thermal carrier transport 13 (2015) 67–76, https://doi.org/10.1016/j.nanoen.2015.02.001.
[35] Q. Zhang, X. Ai, W. Wang, L. Wang, W. Jiang, Preparation of 1-d/3-d structured agnws/bi2te3 nanocomposites with enhanced thermoelectric properties 73 (2014) 37–47, https://doi.org/10.1016/j.actamat.2014.03.070.
[36] B. Madavali, C.-H. Lee, H.-S. Kim, K.-H. Lee, S.-J. Hong, Investigation of microstructure and thermoelectric properties of p-type bisbte /zno composites, Int. J. Appl. Ceram. Technol. 15 (2017), https://doi.org/10.1111/ijac.12789.
[37] Y. Li, Q. Zhao, Y.-G. Wang, K. Bi, Synthesis and characterization of bi2te3/polyaniline composites, Mater. Sci. Semicond. Process. 14 (2011) 219–222, https://doi.org/10.1016/j.mssp.2011.02.019.
[38] Y. Zhang, X.L. Wang, W.K. Yeoh, R.K. Zheng, C. Zhang, Electrical and thermoelectric properties of single-wall carbon nanotube doped bi2te3 (2012) 101, https://doi.org/10.1063/1.4737898.
[39] A. Kaleem, W. Chunlei, Enhanced thermoelectric performance of bi2te3 through uniform dispersion of single wall carbon nanotubes, Nanotechnology 28 (2017) 1, https://doi.org/10.1007/s11664-016-5095-z.
[40] K.T. Kim, S.Y. Choi, E.H. Shin, K.S. Moon, H.Y. Koo, G.-G. Lee, G.H. Ha, The influence of cnts on the thermoelectric properties of a cnt/bi2te3 composite, Carbon 52 (2013) 541–549, https://doi.org/10.1016/j.carbon.2012.10.008.
[41] K. Tae Kim, Y. Seong Eom, I. Son, Fabrication process and thermoelectric properties of cnt/bi2(se,te)3 composites, Journal of Nanomaterials 2015 (2014)
[42] S. Kumar, D. Chaudhary, P.K. Dhawan, R.R. Yadav, N. Khare, Bi2te3-mwcnt nanocomposite: An efficient thermoelectric material, 43 (2017) 14976-14982, 10.1016/j.ceramint.2017.08.017.
[43] H. Bark, J.-S. Kim, H. Kim, J.-H. Yim, H. Lee, Effect of multiwalled carbon nanotubes on the thermoelectric properties of a bismuth telluride matrix, Curr. Appl Phys. 13 (2013) S111–S114, https://doi.org/10.1016/j.cap.2013.01.019.
[44] D.-H. Park, M.-Y. Kim, T.-S. Oh, Thermoelectric energy-conversion characteristics of n-type bi2(te, se)3 nanocomposites processed with carbon nanotube dispersion, Curr. Appl Phys. 11 (2011) S41–S45, https://doi.org/10.1016/j.cap.2011.07.007.
[45] M.Y. Kim, Y.H. Yeo, D.H. Park, T.S. Oh, Thermoelectric characteristics of the (bi, sb)2(te, se)3 nanocomposites processed with nanoparticle dispersion, Ceram. Int. 38 (2012) S529–S533, https://doi.org/10.1016/j.ceramint.2011.05.069.
[46] F. Ren, H. Wang, P.A. Menchhofer, J.O. Kiggans, Thermoelectric and mechanical properties of multi-walled carbon nanotube doped bi0.4sb1.6te3 thermoelectric material, 103 (2013), 10.1063/1.4834700.
[47] Y.H. Yeo, T.S. Oh, Thermoelectric properties of p-type (bi, sb)2te3 nanocomposites dispersed with multiwall carbon nanotubes, Mater. Res. Bull. 58 (2014) 54–58, https://doi.org/10.1016/j.materresbull.2014.04.046.
[48] B. Trawinski, B. Bochentyn, N. Gostkowska, M. Lapinski, T. Miruszewski, B. Kusz, Structure and thermoelectric properties of bismuth telluride-carbon composites 99 (2018) 10–17, https://doi.org/10.1016/j.materresbull.2017.10.043.
[49] K. Ahmad, C. Wan, M. Al-Eshaikh, Effect of uniform dispersion of single-wall carbon nanotubes on the thermoelectric properties of bisbte-based nanocomposites, J. Electron. Mater. 46 (2017) 1348, https://doi.org/10.1007/s11664-016-5095-z.
[50] C.-J. Liu, G.-J. Liu, C.-J. Su, Power factor improvement in hydrothermally synthesized bi2−x sb x te3 (x=1.5) — carbon spheree composites, Journal of Solid State Chemistry 193 (2012) 127–132, https://doi.org/10.1016/j.jssc.2012.05.005.
[51] M. Popov, S. Buga, P. Vysikaylo, P. Stepanov, V. Skok, V. Medvedev, E. Tatyanin, V. Denisov, A. Kirichenko, V. Aksenenkov, V. Blank, C60-doping of nanostructured bi-sb-te thermoelectrics, 208 (2011) 2783-2789, 10.1002/pssa.201127075.
[52] N.W. Gothard, T.M. Tritt, J.E. Spowart, Figure of merit enhancement in bismuth telluride alloys via fullerene-assisted microstructural refinement, J. Appl. Phys. 110 (2011), https://doi.org/10.1063/1.3606547 023706.
[53] V. Kulbachinskiia, V. Kytina, V. Blankb, S. Bugab, M. Popov, Thermoelectric properties of bismuth telluride nanocomposites with fullerene, Semiconductors 45 (2015) 1194–1198.
[54] N. Gothard, J.E. Spowart, T.M. Tritt, Thermal conductivity reduction in fullerene-enriched p-type bismuth telluride composites 207 (2010) 157–162, https://doi.org/10.1002/pssa.200925145.
[55] N. Gothard, G. Wilks, T.M. Tritt, J.E. Spowart, Effect of processing route on the microstructure and thermoelectric properties of bismuth telluride-based alloys 39 (2010) 1909–1913, https://doi.org/10.1007/s11664-009-1051-5.
[56] Y.C. Dou, X.Y. Qin, D. Li, L.L. Li, T.H. Zou, Q.Q. Wang, Enhanced thermopower and thermoelectric performance through energy filtering of carriers in (bi2te3)0.2(sb2te3)0.8 bulk alloy embedded with amorphous sio2 nanoparticles 044906-044906-044906, Journal of Applied Physics 114 (2013), https://doi.org/10.1063/1.4817074.
[57] D.-W. Liu, J.-F. Li, C. Chen, B.-P. Zhang, Effects of sic nanodispersion on the thermoelectric properties of p-type and n-type bi2te3-based alloys 40 (2011) 992–998, https://doi.org/10.1007/s11664-010-1476-x.

[58] J. Li, Q. Tan, J.F. Li, D.W. Liu, F. Li, Z.Y. Li, M. Zou, K. Wang, Bisbte-based nanocomposites with high zt: The effect of sic nanodispersion on thermoelectric properties, Adv. Funct. Mater. 23 (2014) 4317–4323, https://doi.org/10.1002/adfm.201300146.
[59] Y.C. Dou, X.Y. Qin, D. Li, Y.Y. Li, H.X. Xin, J. Zhang, Y.F. Liu, C.J. Song, L. Wang, Enhanced thermoelectric performance of bisbte-based composites incorporated with amorphous si3n4 nanoparticles, 5 (2015) 34251-34256, 10.1039/c5ra04428f.
[60] J.-F. Li, J. Liu, Effect of nano-sic dispersion on thermoelectric properties of bi2te3 polycrystals, 203 (2006) 3768-3773, 10.1002/pssa.200622011.
[61] M.Y. Kim, B.K. Yu, J.Y. Choi, T.S. Oh, Thermoelectric characteristics of the p-type (bi, sb)2te3 nanocomposites processed with silicon nanodispersion, Journal Of Nanoscience And Nanotechnology 14 (2014) 7855–7859, https://doi.org/10.1166/jnn.2014.9421.
[62] Y. Dou, X. Yan, Y. Du, J. Xu, D. Li, Thermoelectric properties of bi0.4sb1.6te3-based composites with silicon nano-inclusions, (2020), 10.1007/s10854-020-03042-1.
[63] K.T. Kim, H.Y. Koo, G.-G. Lee, G.H. Ha, Synthesis of alumina nanoparticle-embedded-bismuth telluride matrix thermoelectric composite powders, Mater. Lett. 82 (2012) 141–144, https://doi.org/10.1016/j.matlet.2012.05.053.
[64] K. Tae Kim, G.H. Ha, Fabrication and enhanced thermoelectric properties of alumina nanoparticle-dispersed bi0.5sb1.5te3 matrix composites, Journal of Nanomaterials 2013 (2013).
[65] B. Madavali, H. Kim, S.-J. Hong, Reduction of thermal conductivity in al2o3 dispersed p-type bismuth antimony telluride composites, Mater. Chem. Phys. 233 (2019) 9–15, https://doi.org/10.1016/j.matchemphys.2019.05.023.
[66] Q. Zhang, X. Ai, L. Wang, Y. Chang, W. Luo, W. Jiang, L. Chen, Improved thermoelectric performance of silver nanoparticles-dispersed bi2te3 composites deriving from hierarchical two-phased heterostructure, Adv. Funct. Mater. 25 (2015) 966–976, https://doi.org/10.1002/adfm.201402663.
[67] S. Cao, Z.-G. Chen, Z.-Y. Huang, J. Xu, L. Yang, F.-Q. Zu, Enhanced thermoelectric properties of ag-modified bi0.5sb1.5te3 composites by a facile electroless plating method, ACS Applied Materials & Interfaces 9 (2017) 36478–36482, https://doi.org/10.1021/2Facsami.7b11989.
[68] G. Yang, R. Niu, L. Sang, X. Liao, D.R.G. Mitchell, N. Ye, J. Pei, J.-F. Li, X. Wang, Ultra-high thermoelectric performance in bulk bisbte/amorphous boron composites with nano-defect architectures, Adv. Energy Mater. 10 (2020) 2000757, https://doi.org/10.1002/aenm.202000757.
[69] Y. Li, X. Wang, G. Liu, B. Shin, F. Shan, High thermoelectric efficiency of p-type bisbte-based composites with cugate2 nanoinclusions, Scr. Mater. 172 (2019) 88–92, https://doi.org/10.1016/j.scriptamat.2019.07.016.
[70] S. Yoon, P. Dharmaiah, H.-S. Kim, C. Lee, S.-J. Hong, J. Koo, Investigation of thermoelectric properties with dispersion of feo and fe-85ni nanospheres in bisbte matrix, J. Electron. Mater. 46 (2017) 2770, https://doi.org/10.1007/s11664-016-4962-y.
[71] L. Xing, W. Cui, X. Sang, F. Hu, P. Wei, W. Zhu, X. Nie, Q. Zhang, W. Zhao, Enhanced thermoelectric performance and atomic-resolution interfacial structures in bisbte thermo-electro-magnetic nanocomposites incorporating magnetocaloric lafesi nanoparticles, J. Materiomics (2021), https://doi.org/10.1016/j.jmat.2021.02.013.
[72] B. Du, X. Lai, Q. Liu, H. Liu, J. Wu, J. Liu, Z. Zhang, Y. Pei, H. Zhao, J. Jian, Spark plasma sintered bulk nanocomposites of bi 2 te 2.7 se 0.3 nanoplates incorporated ni nanoparticles with enhanced thermoelectric performance, ACS Appl. Mater. Interfaces 11 (2019) 31816–31823, https://doi.org/10.1021/acsami.9b08392.
[73] A. Pakdel, Q. Guo, V. Nicolosi, T. Mori, Enhanced thermoelectric performance of bi–sb–te/sb2o3 nanocomposites by energy filtering effect, J. Mater. Chem. A 6 (2018) 21341–21349, https://doi.org/10.1039/C8TA08238C.
[74] E.B. Kim, P. Dharmaiah, D. Shin, K.-H. Lee, S.-J. Hong, Enhanced thermoelectric performance through carrier scattering at spherical nanoparticles in bi0.5sb1.5te3/ta2o5 composites, J. Alloy. Compd. 703 (2017) 614–623, https://doi.org/10.1016/j.jallcom.2017.01.340.
[75] E.B. Kim, P. Dharmaiah, K.-H. Lee, C.-H. Lee, J.-H. Lee, J.-K. Yang, D.-H. Jang, D.-S. Kim, S.-J. Hong, Enhanced thermoelectric properties of bi0.5sb1.5te3 composites with in-situ formed senarmontite sb2o3 nanophase, J. Alloy. Compd. 777 (2019) 703–711, https://doi.org/10.1016/j.jallcom.2018.10.408.
[76] C. Nagarjuna, B. Madavali, L.E.E. Myeong-Won, Y. Suk-Min, H. Soon-Jik, Reduction of thermal conductivity through the dispersion of tic nanoparticles into a p-type bi0.5sb1.5te3 alloy by ball milling and spark plasma sintering, Archives of Metallurgy & Materials 64 (2019) 551-557, 10.24425/amm.2019.127577.
[77] Q. Jiang, J. Yang, J. Xin, Z. Zhou, D. Zhang, H. Yan, Carriers concentration tailoring and phonon scattering from n-type zinc oxide (zno) nanoinclusion in p- and n-type bismuth telluride (bi2te3): Leading to ultra low thermal conductivity and excellent thermoelectric properties, J. Alloy. Compd. 694 (2017) 864–868, https://doi.org/10.1016/j.jallcom.2016.10.076.
[78] I.T. Witting, F. Ricci, T.C. Chasapis, G. Hautier, G.J. Snyder, The thermoelectric properties of -type bismuth telluride: Bismuth selenide alloys, Research 2020 (2020) 15, https://doi.org/10.34133/2020/4361703.
[79] Z.-G. Chen, G. Han, L. Yang, L. Cheng, J. Zou, Nanostructured thermoelectric materials: Current research and future challenge, Progress in Natural Science: Materials International 22 (2012) 535–549, https://doi.org/10.1016/j.pnsc.2012.11.011.
[80] G.C. Dannangoda, C. Key, M. Sumets, K.S. Martirosyan, Transition of p- to n-type conductivity in mechanically activated bismuth telluride, J. Electron. Mater. 47 (2018) 5800–5809, https://doi.org/10.1007/s11664-018-6469-1.
[81] M. Siddiqui, A.F. Arif, Generalized effective medium theory for particulate nanocomposite materials, Materials 9 (2016) 694, https://doi.org/10.3390/ma9080694.
[82] J. Payandehpeyman, M. Mazaheri, M. Khamehchi, Prediction of electrical conductivity of polymer-graphene nanocomposites by developing an analytical model considering interphase, tunneling and geometry effects, Compos. Commun. 21 (2020), https://doi.org/10.1016/j.coco.2020.100364 100364.
[83] S.I. Ahmad, H. Hamoudi, J. Ponraj, K.M. Youssef, In-situ growth of single-crystal plasmonic aluminum–lithium-graphene nanosheets with a hexagonal platelet-like morphology using ball-milling, Carbon 178 (2021) 657–665, https://doi.org/10.1016/j.carbon.2021.03.053.
[84] Y. Zare, K.Y. Rhee, Simulation of percolation threshold, tunneling distance, and conductivity for carbon nanotube (cnt)-reinforced nanocomposites assuming effective cnt concentration, Polymers 12 (2020) 114, https://doi.org/10.3390/polym12010114.
[85] G.-H. Gwak, M.-K. Kim, W.-J. Lee, D.-G. Jeung, J.K. Park, S.-M. Paek, J.-M. Oh, Facile synthetic route to prepare ultrathin silver nanosheets by reducing silver thiolates in interlayer surface of layered double hydroxides, Inorg. Chem. 59 (2020) 2163–2170, https://doi.org/10.1021/acs.inorgchem.9b02694.
[86] T. Wejrzanowski, M. Grybczuk, M. Chmielewski, K. Pietrzak, K.J. Kurzydlowski, A. Strojny-Nedza, Thermal conductivity of metal-graphene composites, Mater. Des. 99 (2016) 163–173, https://doi.org/10.1016/j.matdes.2016.03.069.
[87] K. Chu, X.-H. Wang, Y.-B. Li, D.-J. Huang, Z.-R. Geng, X.-L. Zhao, H. Liu, H. Zhang, Thermal properties of graphene/metal composites with aligned graphene, Mater. Des. 140 (2018) 85–94, https://doi.org/10.1016/j.matdes.2017.11.048.
[88] J. Ren, Q. Li, L. Yan, L. Jia, X. Huang, L. Zhao, Q. Ran, M. Fu, Enhanced thermal conductivity of epoxy composites by introducing graphene@boron nitride nanosheets hybrid nanoparticles, Mater. Des. 191 (2020), https://doi.org/10.1016/j.matdes.2020.108663 108663.
[89] F. Zhang, J. Wang, T. Liu, C. Shang, Enhanced mechanical properties of few-layer graphene reinforced titanium alloy matrix nanocomposites with a network architecture, Mater. Des. 186 (2020), https://doi.org/10.1016/j.matdes.2019.108330 108330.
[90] C. Shang, F. Zhang, B. Zhang, F. Chen, Interface microstructure and strengthening mechanisms of multilayer graphene reinforced titanium alloy matrix nanocomposites with network architectures, Mater. Des. 196 (2020), https://doi.org/10.1016/j.matdes.2020.109119 109119.
[91] X.-J. Shen, C.-Y. Dang, B.-L. Tang, X.-H. Yang, H.-J. Nie, J.-J. Lu, T.-T. Zhang, K. Friedrich, The reinforcing effect of oriented graphene on the interlaminar shear strength of carbon fabric/epoxy composites, Mater. Des. 185 (2020), https://doi.org/10.1016/j.matdes.2019.108257 108257.
[92] A.K. Bohra, R. Bhatt, A. Singh, S. Bhattacharya, R. Basu, K.N. Meshram, S.K. Sarkar, P. Bhatt, P.K. Patro, D.K. Aswal, K.P. Muthe, S.C. Gadkari, Transition from n- to p-type conduction concomitant with enhancement of figure-of-merit in pb doped bismuth telluride: Material to device development, Mater. Des. 159 (2018) 127–137, https://doi.org/10.1016/j.matdes.2018.08.035.
[93] L. Wei, X. Liu, Y. Gao, X. Lv, N. Hu, M. Chen, Synergistic strengthening effect of titanium matrix composites reinforced by graphene oxide and carbon nanotubes, Mater. Des. 197 (2021), https://doi.org/10.1016/j.matdes.2020.109261 109261.
[94] A. Zolriasatein, X. Yan, E. Bauer, P. Rogl, A. Shokuhfar, S. Paschen, Influence of pca on thermoelectric properties and hardness of nanostructured ba–cu–si clathrates, Mater. Des. 87 (2015) 883–890, https://doi.org/10.1016/j.matdes.2015.08.096.
[95] M. Aureli, C.C. Doumanidis, I.E. Gunduz, A.G.S. Hussien, Y. Liao, N. Kostoglou, C. Rebholz, C.C. Doumanidis, Bimetallic diffusion modeling and temperature regulation during ball milling, Mater. Des. 155 (2018) 233–243, https://doi.org/10.1016/j.matdes.2018.05.055.
[96] B. Cai, H.-L. Zhuang, J. Pei, B. Su, J.-W. Li, H. Hu, Y. Jiang, J.-F. Li, Spark plasma sintered bi-sb-te alloys derived from ingot scrap: Maximizing thermoelectric performance by tailoring their composition and optimizing sintering time, Nano Energy 85 (2021), https://doi.org/10.1016/j.nanoen.2021.106040 106040.
[97] A. Nozariasbmarz, F. Suarez, J.H. Dycus, M.J. Cabral, J.M. LeBeau, M.C. Öztürk, D. Vashaee, Thermoelectric generators for wearable body heat harvesting: Material and device concurrent optimization, Nano Energy 67 (2020), https://doi.org/10.1016/j.nanoen.2019.104265 104265.
[98] Z.-Y. Hu, Z.-H. Zhang, X.-W. Cheng, F.-C. Wang, Y.-F. Zhang, S.-L. Li, A review of multi-physical fields induced phenomena and effects in spark plasma sintering: Fundamentals and applications, Mater. Des. 191 (2020), https://doi.org/10.1016/j.matdes.2020.108662 108662.
[99] F.F. Jaldurgam, Z. Ahmad, F. Touati, A.A. Ashraf, A. Shakoor, J. Bhadra, N.J. Al-Thani, D.S. Han, T. Altahtamouni, Optimum sintering method and temperature for cold compact bismuth telluride pellets for thermoelectric applications, J. Alloy. Compd. 877 (2021), https://doi.org/10.1016/j.jallcom.2021.160256 160256.
[100] M.H. Lee, J.H. Park, S.-D. Park, J.-S. Rhyee, M.-W. Oh, Grain growth mechanism and thermoelectric properties of hot press and spark plasma sintered na-doped pbte, J. Alloy. Compd. 786 (2019) 515–522, https://doi.org/10.1016/j.jallcom.2019.01.387.